Scientific Research Publishing

Computational Water, Energy, and Environmental Engineering, 2023, 12, 27-57
https://www.scirp.org/journal/cweee
ISSN Online: 2168-1570
ISSN Print: 2168-1562

The Hydrodynamic Behaviour of Euboean Gulf Coastal Areas and the Mixing of the Physico-Chemical Characteristics of Urban Sewage Discharged into Them under the Influence of Climate Change

Evangelos Tsirogiannis, Panagiotis Angelidis

Division of Hydraulics, Department of Civil Engineering, School of Engineering, Democritus University of Thrace, Kimmeria Campus, Xanthi, Greece
Email: pangelid@civil.duth.gr, eva.tsirogiannis@gmail.com

How to cite this paper: Tsirogiannis, E. and Angelidis, P. (2023) The Hydrodynamic Behaviour of Euboean Gulf Coastal Areas and the Mixing of the Physico-Chemical Characteristics of Urban Sewage Discharged into Them under the Influence of Climate Change. *Computational Water, Energy, and Environmental Engineering*, **12**, 27-57.
https://doi.org/10.4236/cweee.2023.124002

Received: September 3, 2023
Accepted: October 24, 2023
Published: October 27, 2023

Abstract

The hydrodynamic circulation within the marine environment is a complex phenomenon, characterized by the interplay of strong tidal forces, atmospheric influences, and bathymetric features. The physical and hydrodynamic attributes of this flow play a pivotal role in promoting vertical mixing of seawater masses, thereby facilitating the integration of their physical and chemical parameters, including nutrients and oxygen. Additionally, they are instrumental in governing the dispersion and diffusion of pollutants originating from urban sewage, contributing to the overall water renewal process and environmental quality. This study investigates the potential impact of anticipated increases in average air temperatures on water column stratification in coastal regions susceptible to these dynamic influences. These areas receive treated urban sewage, and the study aims to assess how these temperature changes might influence the dispersion and mixing of pollutant loads present in these coastal waters.

Keywords

Hydrodynamic Modeling, Climate Change, Euboean Gulf Greece, Stratification, Sewage Mixing, Water Quality Modeling

1. Introduction

The hydrodynamic circulation in coastal systems is intricately influenced by a

variety of interacting factors, including tides, waves, and river inflows. Numerous researchers have devoted their efforts to modeling the impacts of tidal forces [1]-[6]. These hydrodynamic processes play a significant role in shaping the dispersion and transport of pollutants within coastal waters. Furthermore, tidal currents have the propensity to oscillate pollutants back and forth, occasionally leading to their dispersion into the open sea [7].

In the Eastern Mediterranean region, tidal currents are generally characterized by their relatively weak and often low-speed nature [8]. One of the earliest documented instances of tidal phenomena dates back to observations made in the Euboean Gulf (Greece) by historical figures such as Eratosthenes, Pitheas, Posidonios [9], Stravon, and Senekas [10], with subsequent studies conducted by researchers in the early 20th century [9]-[14]. While certain research endeavors have explored sea level changes in the broader southern European region [15] [16] [17] [18], including the Euboean Gulf [19] [20], systematic measurements and comprehensive literature describing, elucidating, and illustrating the manifold effects of tides on hydrodynamic circulation, as well as their influence on pollutant diffusion and transport, remain relatively scarce [21].

In this study, we employed computer simulation to model the hydrodynamic circulation within the Euboean Gulf region. We utilized the AEM3D (3-Dimensional coupled Hydrodynamic-Aquatic Ecosystem Model), an evolution of the ELCOM-CAEDYM software, known for its effectiveness in simulating hydrodynamic models encompassing various factors. These factors include the strong tides characteristic of the study area, the Coriolis force resulting from Earth's rotation, and meteorological variables such as total solar radiation, atmospheric pressure, relative humidity, precipitation, air temperature, wind speed, and direction. The AEM3D model has also been successfully applied in numerous studies worldwide, including investigations in the North Aegean Sea [22] [23], the Adriatic Sea [24], the Persian Gulf [25], as well as a study encompassing tidal simulations in Blagdon Lake, UK, and an exploration of the impact of climate change on stratification with mitigation measures [26]. In the context of this work, special research pertaining to the hydrodynamic state of the Euboean Gulf and the factors influencing it have been carried out by Kotsovinos and Skaloumpakas [27] [28]. Furthermore, the Mixing Characteristics under Tide, Mereological, and Oceanographic Conditions in the Euboean Gulf [29] were simulated in a recent study by the author, utilizing the AEM3D model. Additionally, the water circulation in the North and South Evoikos Gulfs was simulated in a recent study by the authors [21], employing the AEM3D model, akin to the previous investigation, the Mixing Characteristics under Tide, Mereological, and Oceanographic Conditions in the Euboean Gulf [29]. According to data from the official COPERNICUS climate change services system (https://climate.copernicus.eu), the average global air temperature has increased by 1.21˚C from pre-industrial times (1970-2022). Projections indicate an additional 0.29˚C increase by the year 2034, resulting in an expected average air temperature increase of 1.5˚C in contrast to 1970, as depicted in **Figure 1** below.

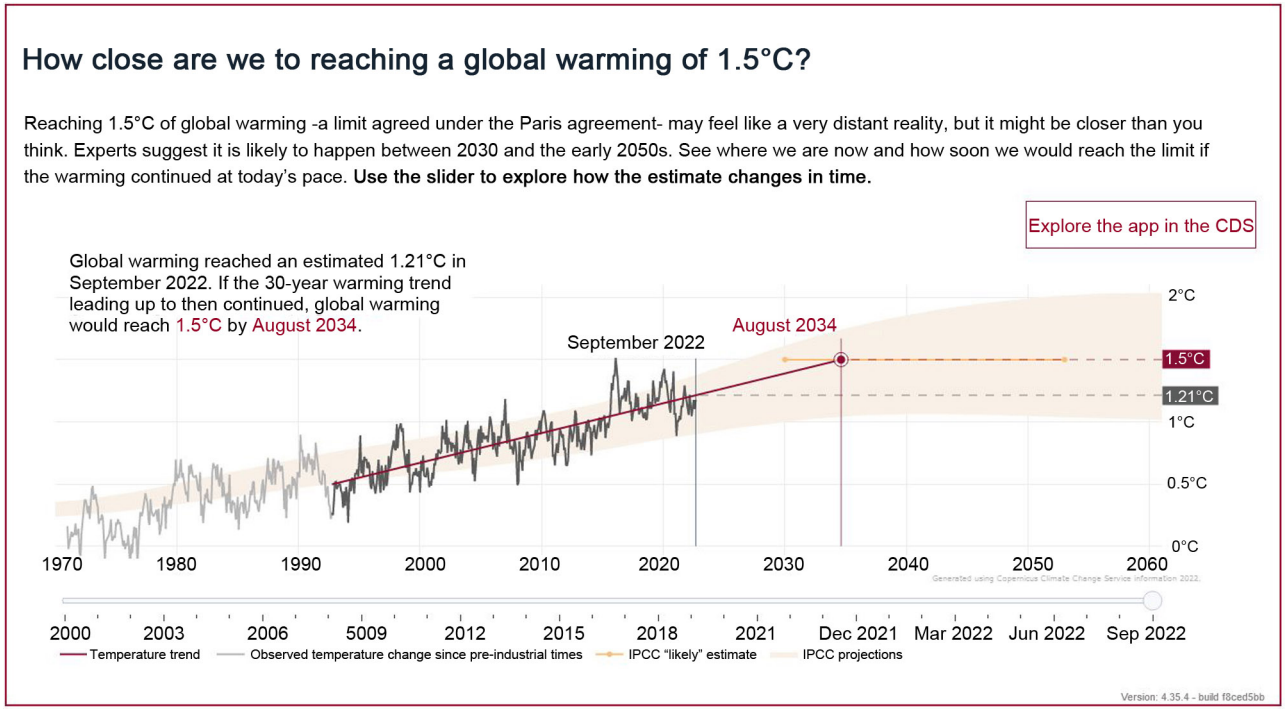

Figure 1. Increase in average global air temperature from the year 1970 to the year 2034, obtained from the official website: https://climate.copernicus.eu.

In this study, we contemplate a theoretical climate scenario wherein the global air temperature is projected to increase by 1.5˚C in the future. This assumption is based on the premise that the greenhouse effect, which is primarily responsible for this temperature rise, will persist over the next 64 years, causing the average air temperature to continue its upward trajectory at the same historical rate.

The objective of this scenario, as well as our present investigation, is to simulate the anticipated rise in mean air temperature. This simulation aims to assess whether there will be heightened stratification at specific control points within coastal regions of interest in the future. Our goal is to examine the potential impact of this increased stratification on the hydrodynamic conditions in the lower layers of these coastal areas, including parameters such as water temperature, flow velocity, and water renewal times. These hydrodynamic attributes are of paramount importance as they directly influence the vertical mixing of seawater masses, thus affecting the integration of their physical and chemical characteristics, including nutrients and oxygen. Moreover, they play a crucial role in the dispersion of urban sewage originating from simulated disposal pipelines within the computational domain of our study.

2. Methods

2.1. Area of Study

The study area, as depicted in **Figure 2**, encompasses the North Euboean Gulf,

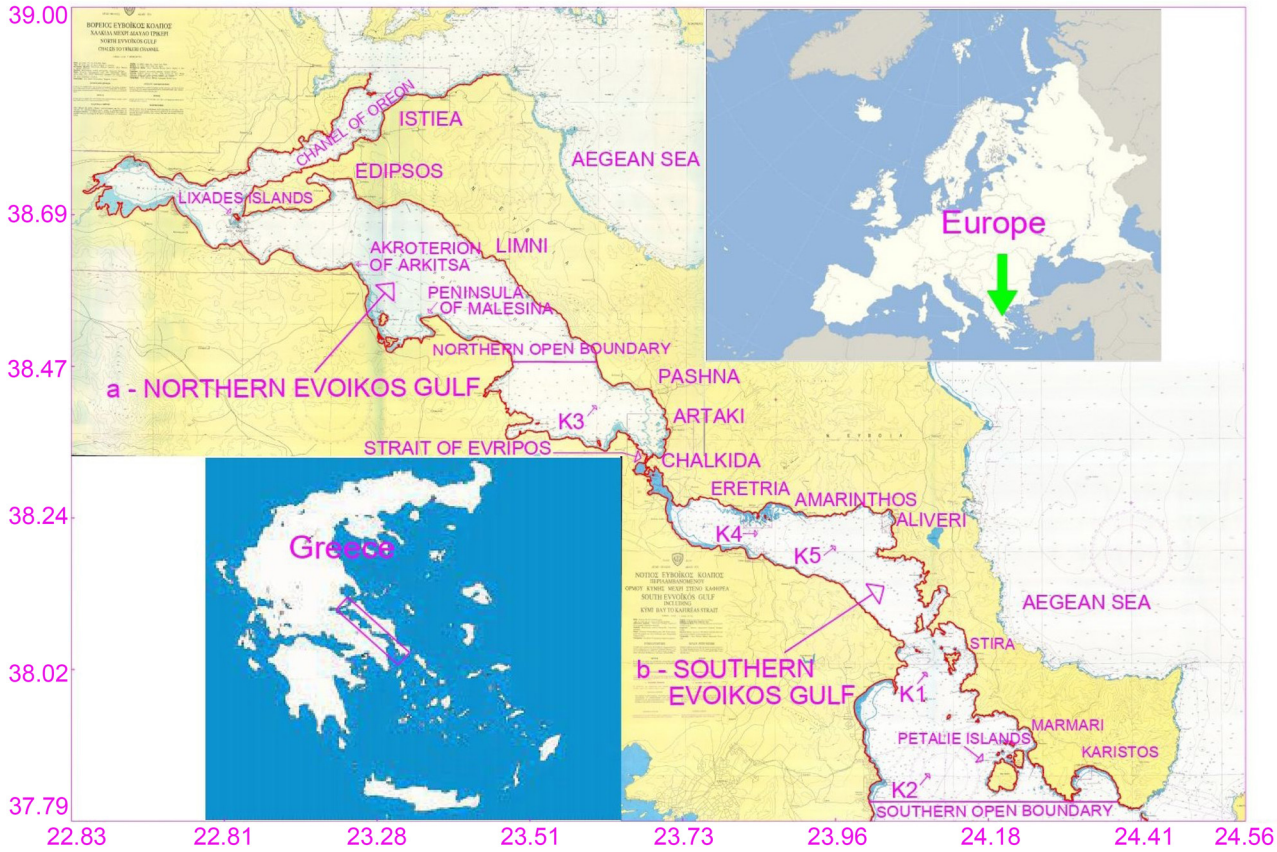

Figure 2. Map of the northern and the southern Gulf of Evoikos.

spanning a total area of 1060 square kilometers, and the South Euboean Gulf, covering an area of 900 square kilometers. These two gulfs are interconnected via the Strait of Euripus, which represents a relatively narrow channel measuring 40 meters in length, 40 meters in width, and with a depth of approximately 10 meters. The defining characteristic of the Strait of Euripus is the presence of robust tidal activity [20]. Typically, during half of the tidal cycle (T/2 = 6 hours), the maximum flow velocity within the Euripus Strait reaches approximately 2.5 meters per second [27] [28].

2.2. Model Configuration

The area chosen for the numerical simulation in this study in the Euboean Gulf, and its bathymetry is illustrated in **Figure 3**. This region is bordered to the west by Central Greece-Attica, to the east by the region of Evia, and to the north and south by the northern and southern Aegean Sea, respectively. For the numerical simulation, we created a rectangular computational grid with variable dimensions. This grid was structured using computational discretization cells ranging from 40 meters by 100 meters to 400 meters by 400 meters. The gradual increase in cell dimensions was necessitated by the narrow 40-meter width of the Euripus Strait on one hand and the need to prevent an excessive number of cells on the other hand. Selecting a grid with fixed dimensions of 40 meters by 40 meters

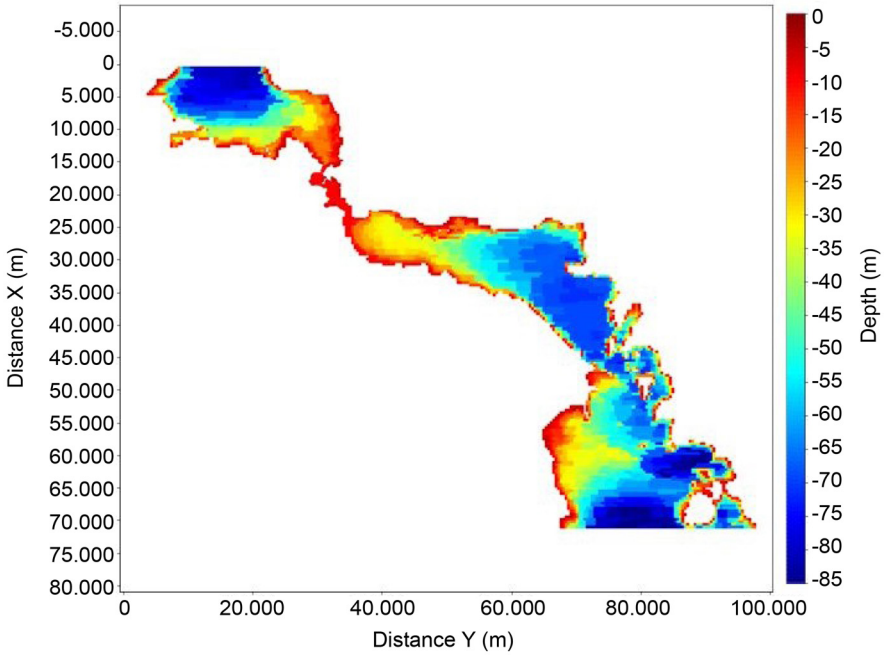

Figure 3. Bathymetric map illustrating the simulation area of the Euboean Gulf.

would have rendered the execution of the computational code infeasible. Consequently, due to this limitation, the computational simulation encompassed the entire South Euboean Gulf and one-third of the North Euboean Gulf. The open boundaries (north and south) of the simulated area are depicted in Figure 2.

We established a total of 20 water layers in the vertical direction for our simulation. The initial eight layers, starting from the surface, exhibited variable thickness ranging from 2.5 meters to 5.0 meters, with a gradual increase. The remaining 13 deeper layers, extending to the bottom, had a consistent thickness of 5.0 meters throughout. We adopted this vertical discretization approach for several reasons:

1) To accurately replicate the hydrodynamic circulation within the 10-meter deep Euripus Strait, a critical factor for the communication between the northern and southern regions of the Euboean Gulf.

2) To provide a more precise representation of results in coastal areas with shallower depths, which are of specific interest.

3) To achieve the highest possible precision in modeling the vertical distribution of velocities, density stratification, and the distribution of contaminants by depth. The maximum depth of our simulation reached −86.0 meters, as indicated in Figure 3, and the total computational domain comprised 225,351 active water cells.

We employed a turbulent benthos-type boundary condition at the bottom, through application of a constant friction coefficient. Additionally, we implemented an "open" boundary condition at the northern and southern boundaries of the computational domain, allowing water to passively flow in or out of each cell based on flow requirements. For the tide simulation, we imposed varying sea

level boundary conditions at the northern and southern boundaries, as illustrated in Figure 4. These conditions were determined based on observations and measurements reported in existing literature [14] [21] [27] [28].

At the commencement of the simulation, the initial salinity and temperature conditions were uniformly set to 38.88 practical salinity units (psu) and 18.35 degrees Celsius (˚C), respectively, for all cells within the computational domain. These values were derived from average data recorded for the year 2016, obtained from the COPERNICUS system. The simulation operated with a time step of 1.0 minute between computational cycles. The initial simulation covered a one-year period, specifically the year 2016, chosen to represent a typical and representative year. Meteorological information, including wind speed and direction, atmospheric pressure, air temperature, relative humidity, rainfall, and solar radiation, was input at 10-minute intervals. This meteorological data, illustrated in Figure 5, was collected from meteorological stations operated by the National Meteorological Service, strategically located in the cities of Lamia and Aliarto, situated adjacent to the area of study.

3. Reliability and Validation

The reliability of the finding in this study has been established, since the hydrodynamic model and the water quality model from which the results have been derived have been tested for reliability. In particular, comparisons have been performed between salinity and water temperature values at various depths of characteristic points of the Euboean Gulf, obtained at various times, from the simulation employing the AEM3D software, and available COPERNICUS model predictions, which resulted in a satisfactory convergence [21].

Similar comparisons have been performed for chlorophyll-a (Chla) at various points on the surface of the Euboean gulf, which have also resulted in satisfactory degree of convergence [29].

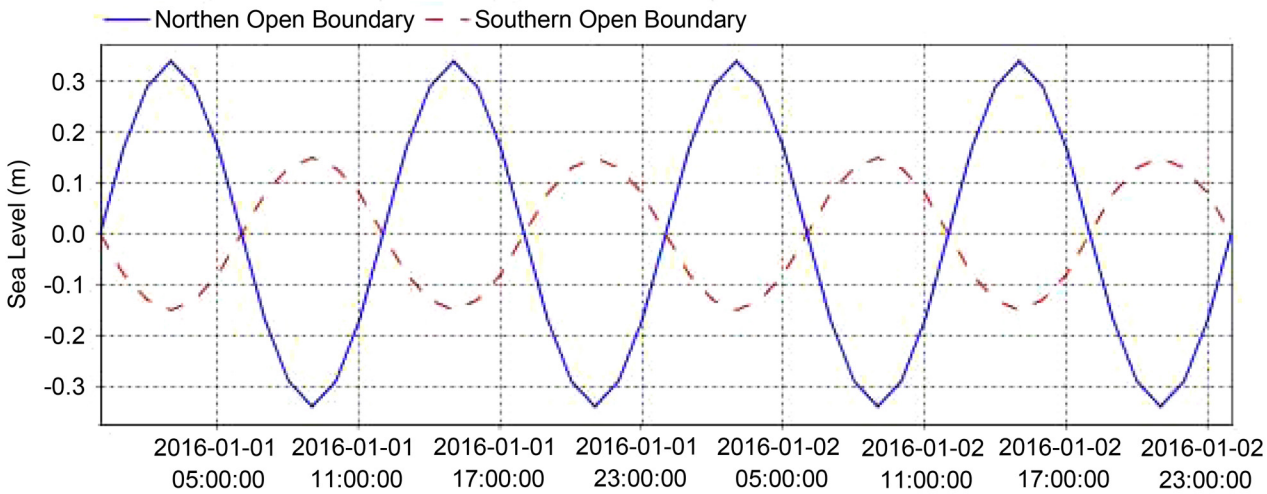

Figure 4. Illustration representing tidal sea level variations at the northern and southern boundaries of the computational domain over a 48-hour period.

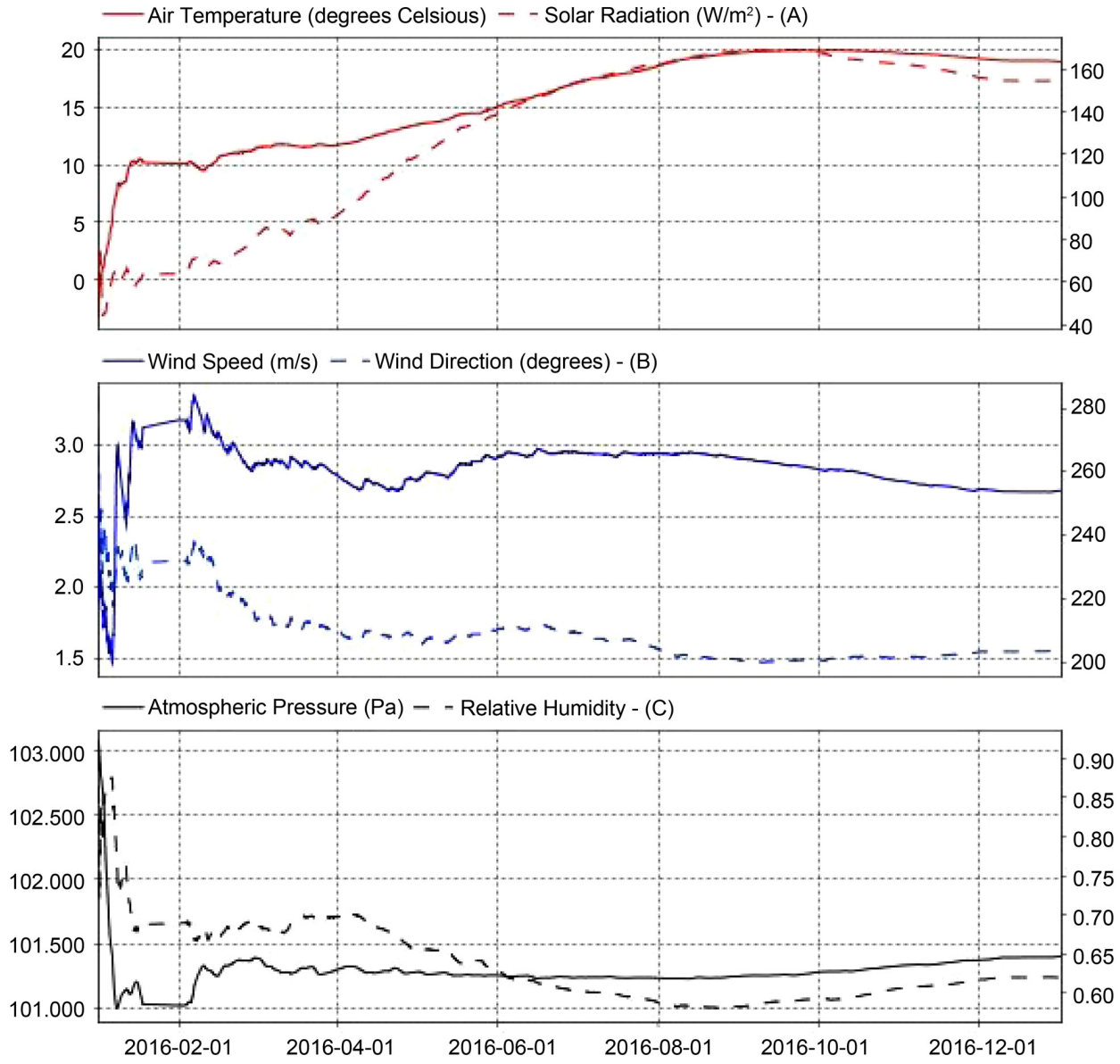

Figure 5. Sub-figures presenting meteorological data recorded every 10 minutes for the year 2016 in the study area. This includes (A) air temperature and solar radiation; (B) wind speed and direction; and (C) atmospheric pressure and relative humidity.

4. Domestic Sewage Discharged in the Region

Five (5) subsea pipelines have been installed for the discharge of treated urban liquid sewage through diffusers within the study area [29]. **Table 1** provides information on the diffuser names, disposal depth, liquid waste flow rates, and initial concentrations of suspended solids, ammonia nitrogen, nitrate nitrogen, phosphate, and total coliforms. In **Figure 6**, you can see the locations of these subsea pipelines and diffusers, along with some control points (P1, P2, P3, P4, P5) defined within the scope of this research. **Figure 7** presents in color the dimensionless concentration of conservative tracers representing the liquid urban waste discharged by the diffusers at various time points during the simulation at

Table 1. Attributes related to the discharge of treated municipal wastewater using diffusers.

No	Diffuser's name	Disposal depth (m)	Urban waste flow (m^3/s)	Concentration of suspended solid particles (mg/l)	BOD (mg/L)	NH_4-N (mg/L)	NO_3-N (mg/L)	PO_4 (mg/L)	Total Coliforms (FC/100ml)
1	DIFFUSER1	18	0.04	10	10	2	11	2	500
2	DIFFUSER2	10	0.24	35	25	15	20	2	500
3	DIFFUSER3	24	0.04	35	25	2	13	10	500
4	DIFFUSER4	19	0.03	30	25	2	13	10	500
5	DIFFUSER5	47	0.04	25	20	2	8	4	500

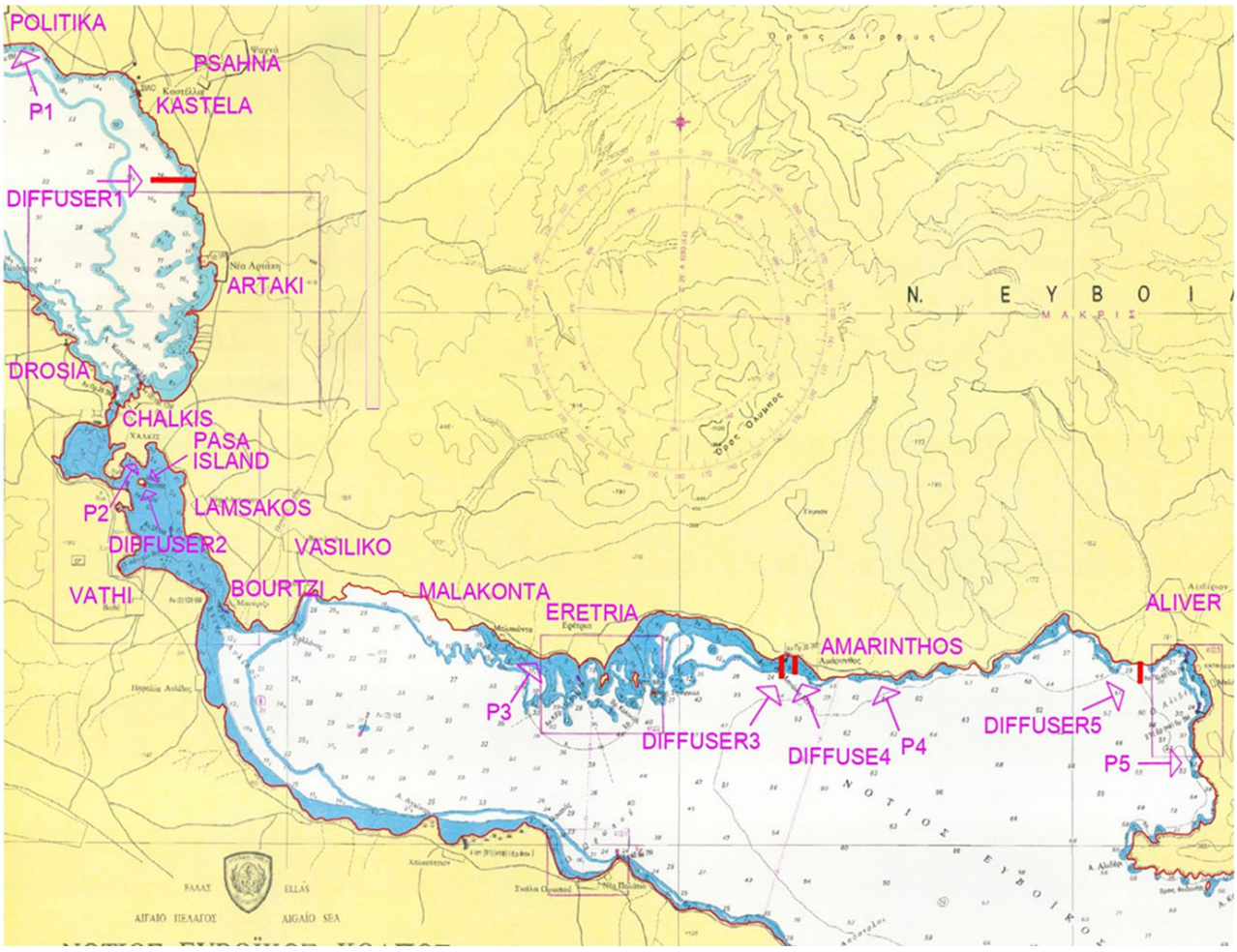

Figure 6. Visual representation depicting the positions of underwater urban wastewater disposal pipelines within the Euboean Gulf, along with the identification of designated control sites situated in the coastal areas, illustrated on a 1:100.000 scale map.

the seabed of these points. Notably, different color scales have been used in the subfigures of Figure 7 to represent sewage diffusion from various discharge flows, as detailed in Table 1. This approach ensures that the diffusion patterns of smaller urban sewage flows are distinguishable.

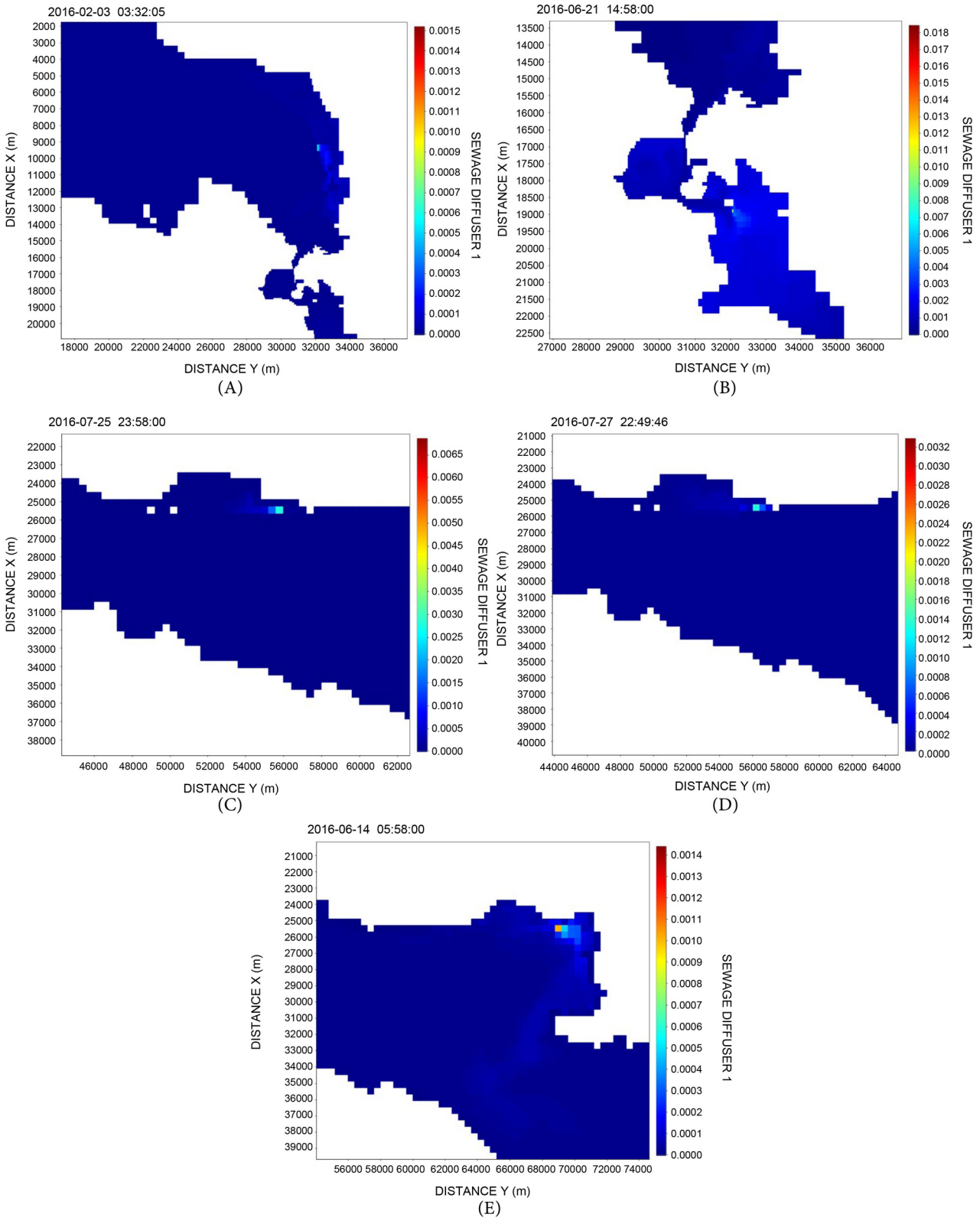

Figure 7. Color-coded representation displaying the dimensionless concentration of preservative tracers originating from urban liquid sewage treatment at various times on the seabed. This includes data from DIFFUSER1 (A) at the time: 2016-02-03-03:32 a.m., DIFFUSER2; (B) at the time: 2016-06-21-14:58 p.m., DIFFUSER3; (C) at the time: 2016-07-25-23:58 p.m., DIFFUSER4; (D) at the time: 2016-07-27-22:50 p.m.; and DIFFUSER5 (E) at the time: 2016-06-14-05:58 a.m.

5. Hypothetical Climate Scenario

In this study, we have considered a theoretical climate scenario involving a projected increase in the average global air temperature by 1.5˚C in the future. This projection is based on the assumption that over the next 64 years, there will not be a significant reduction in greenhouse gas emissions to counteract this phenomenon, which is primarily responsible for the observed temperature rise. Moreover, we anticipate that the average air temperature will continue to rise at the same rate as in previous years, as detailed in the first paragraph. Consequently, we conducted a second simulation in which we modified the meteorological data, specifically adjusting the time series of air temperature values to be consistently 1.5˚C higher than those recorded in 2016, as demonstrated in Figure 8. It's noteworthy that we did not make any alterations to the values of the time series related to incident solar radiation. This decision was influenced by the challenge of predicting changes in cloud cover due to the long-term release of CO_2 and other greenhouse gases, which could potentially influence solar radiation levels.

In the two simulations conducted, one representing the year 2016 and the other depicting the theoretical climate setting, we have identified the warmest period extending from June 15th to August 27th. The peak of this warm period occurred on August 2nd, with a recorded high temperature of 36˚C. During this warm period, we intend to examine the vertical distribution of temperature and water density at all five specified coastal control points of interest (P1, P2, P3, P4, and P5) on August 2nd, which marks the hottest day in the simulations. The purpose of this examination is to investigate whether the anticipated future increase in average air temperature will lead to variations in water column stratification at these points. Consequently, we aim to assess whether such variations

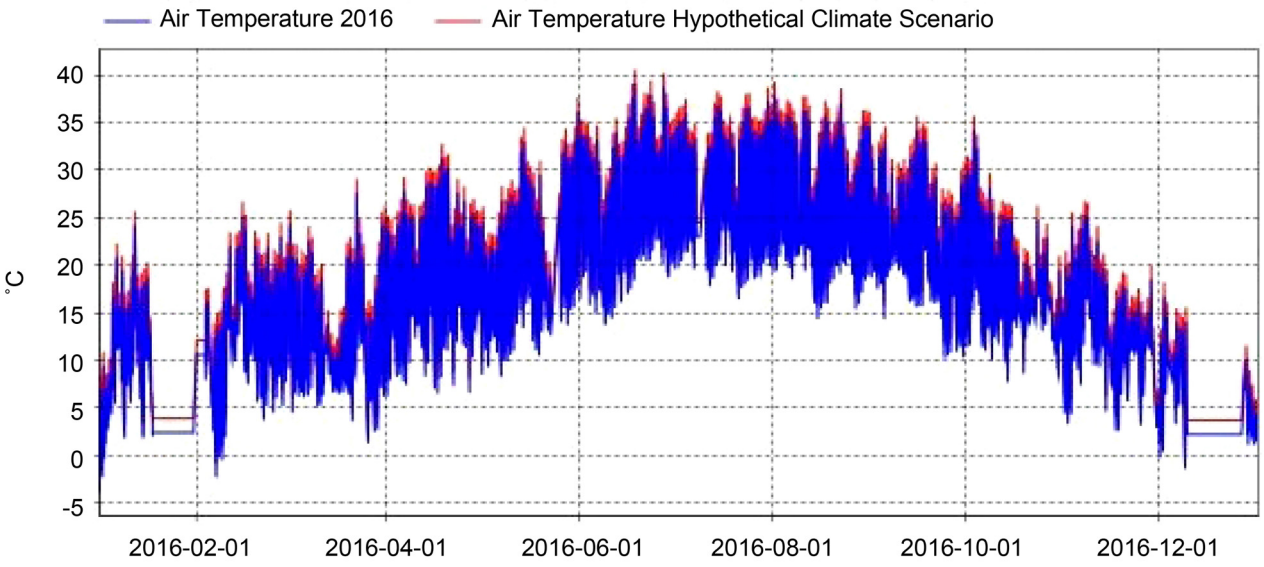

Figure 8. An evaluation comparing the air temperature per decade in the study area between the base year 2016 and a simulated scenario with a 1.5˚C temperature increase, as outlined in the theoretical climate setting.

might have implications for the diffusion of urban wastewater and its pollutants from local disposal pipelines.

6. Results

Based on the comparison of the vertical temperature and water density distributions from the simulation results of the two models, conducted on August 2nd (the warmest day of the simulations) for the five control points (P1, P2, P3, P4, and P5), as depicted in **Figure 9**, it was observed that in most cases, there was an increase in water column stratification:

1) At point P1, as illustrated in **Figure 9(A)**, it is evident that in the speculative climate setting (in comparison to the base year 2016), there is a noticeable steeper slope in both the temperature and water density curves within the water layers ranging from 4 meters to 8 meters from the surface level. However, there is a consistent and uniform change in the thermocline within the seabed layers, specifically from 13 meters to 17 meters.

2) At P2, as illustrated in **Figure 9(B)**, there is an almost uniform distribution in temperature and water density change, across the water column, between the two climate scenarios.

3) At point P3 as illustrated in **Figure 9(C)**, there is a strong variation of the thermocline and the water density curve with height, in the bottom layers from 3.8 m to 8 m, where in the theoretical climate setting, the gradients are more pronounced in comparison to those of the year 2016. Specifically, in these water layers, there is a temperature increase of 1.3˚C per unit height and a 0.25 Kg/m^3 per unit height change in water density, in the theoretical climate setting, in comparison with that of the base year 2016.

4) At point P4 as shown in **Figure 9(D)**, there is little variation in the thermocline and the curve of the vertical distribution of water density in the water layers from 3.5 m from the surface to the bottom. The thermocline is slightly more pronounced in the theoretical climate setting in comparison with the base year 2016. In particular, changes in temperature rise and density in the water column of 0.03˚C and 0.013 Kg/m^3 are observed, respectively.

5) Finally, at P5 as shown in **Figure 9(E)**, there is an increase in both the thermocline and the change in water column density from the water layer 3.6 m from the surface to the bottom. The thermocline is more pronounced in the speculative climate setting than in 2016. Specifically, the change in temperature rise in the water column is of the order of 0.70˚C and in water density 0.40 Kg/m^3.

The uniform distribution of water column stratification observed at point P2, set in the CHALKIS region, is consistent in both climate scenarios. This location places point P2 much closer to the Euripus Strait in comparison to the other control points. The Euripus Strait experiences strong tidal conditions with notably higher water velocities. This is clearly illustrated in **Figure 10**, which shows the change in average water velocity during the warm period from June 15th to

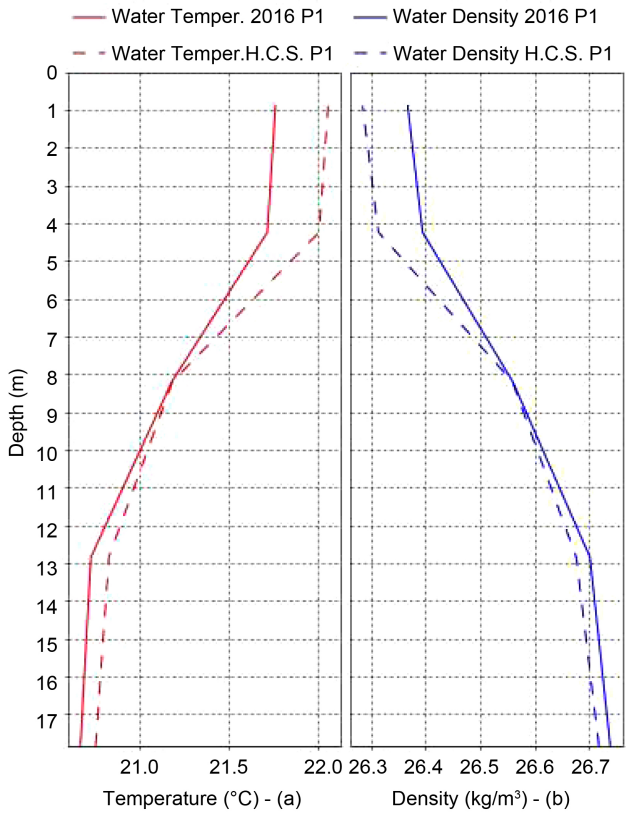
Water Temper. 2016 P1
Water Density 2016 P1
Water Temper.H.C.S. P1
Water Density H.C.S. P1
Depth (m)
0
1
2
3
4
5
6
7
8
9
10
11
12
13
14
15
16
17
21.0
21.5
22.0
26.3
26.4
26.5
26.6
26.7
Temperature (°C) - (a)
Density (kg/m³) - (b)

(A)

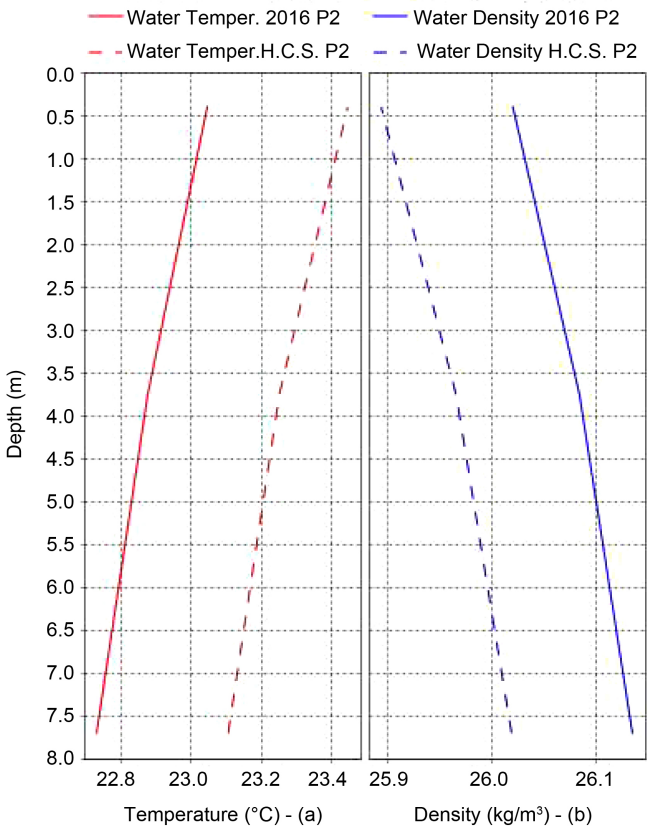
Water Temper. 2016 P2
Water Density 2016 P2
Water Temper.H.C.S. P2
Water Density H.C.S. P2
Depth (m)
0.0
0.5
1.0
1.5
2.0
2.5
3.0
3.5
4.0
4.5
5.0
5.5
6.0
6.5
7.0
7.5
8.0
22.8
23.0
23.2
23.4
25.9
26.0
26.1
Temperature (°C) - (a)
Density (kg/m³) - (b)

(B)

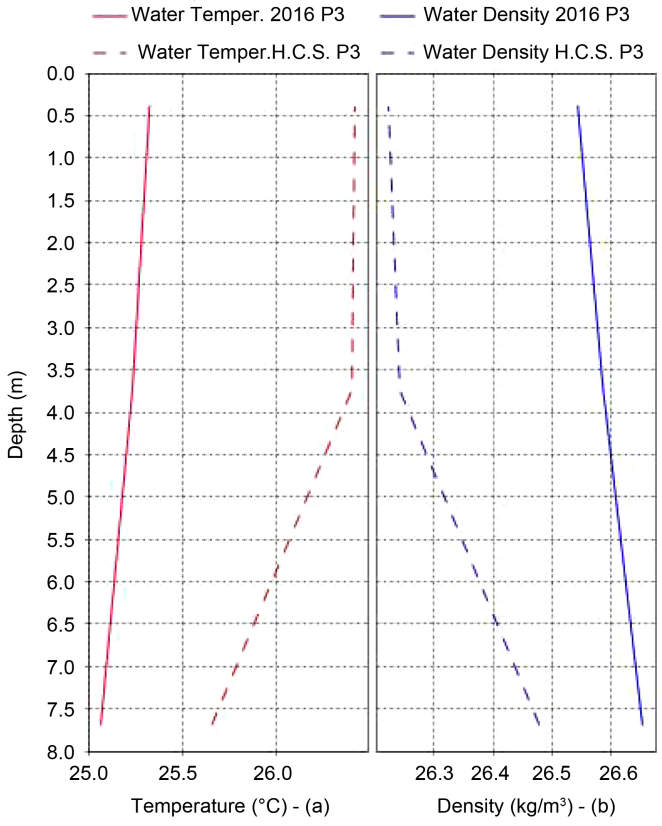
Water Temper. 2016 P3
Water Density 2016 P3
Water Temper.H.C.S. P3
Water Density H.C.S. P3
Depth (m)
0.0
0.5
1.0
1.5
2.0
2.5
3.0
3.5
4.0
4.5
5.0
5.5
6.0
6.5
7.0
7.5
8.0
25.0
25.5
26.0
26.3
26.4
26.5
26.6
Temperature (°C) - (a)
Density (kg/m³) - (b)

(C)

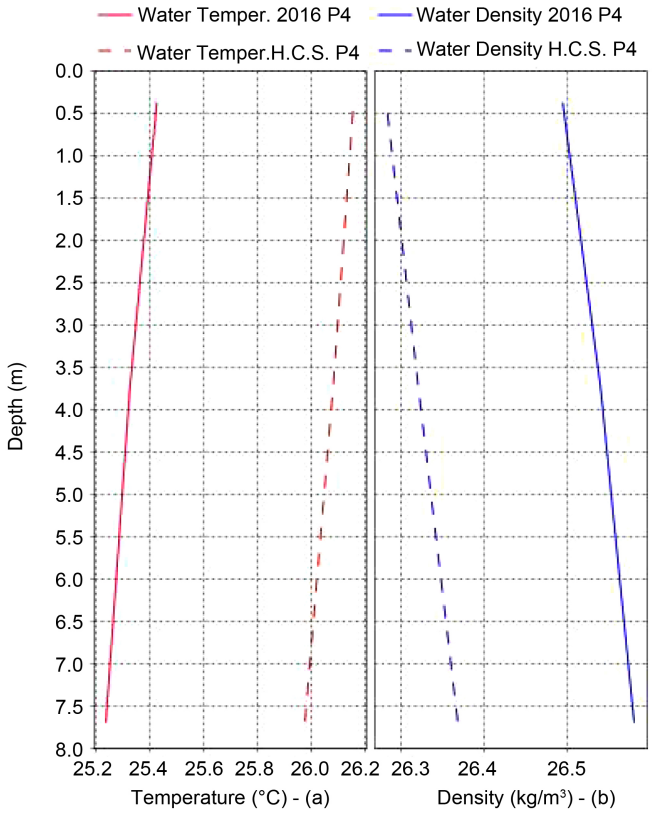
Water Temper. 2016 P4
Water Density 2016 P4
Water Temper.H.C.S. P4
Water Density H.C.S. P4
Depth (m)
0.0
0.5
1.0
1.5
2.0
2.5
3.0
3.5
4.0
4.5
5.0
5.5
6.0
6.5
7.0
7.5
8.0
25.2
25.4
25.6
25.8
26.0
26.2
26.3
26.4
26.5
Temperature (°C) - (a)
Density (kg/m³) - (b)

(D)

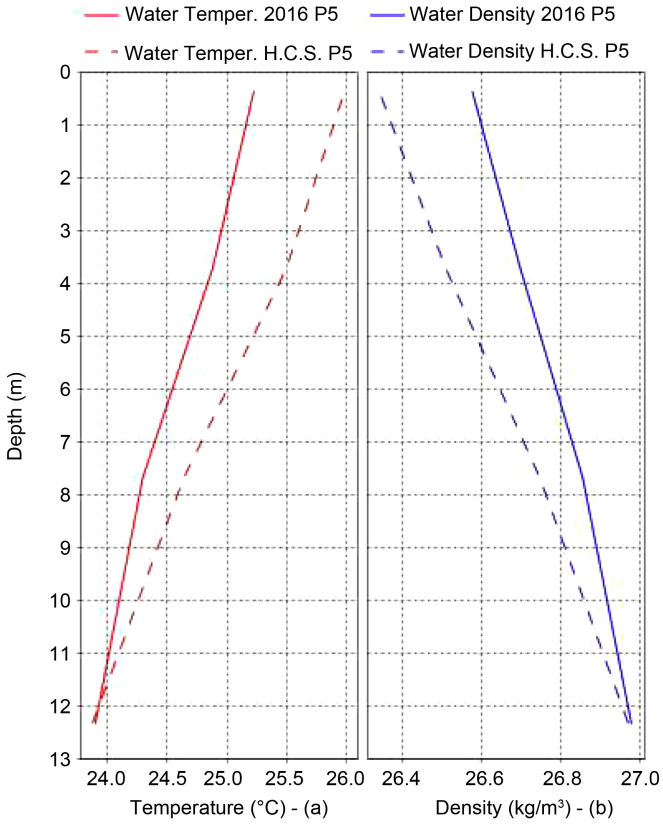

(E)

Figure 9. A comparative analysis of the vertical distribution of (a) Temperature in (˚C) and (b) Water density σ in (Kg/m³), as calculated using the AEM3D software, for both the year 2016 and the hypothetical climate scenario (abbreviated as H.C.S.). Data is presented at (A) Point P1 in the POLITIKA area; (B) Point P2 in the CHALKIS area; (C) Point P3 in the ERETRIA area; (D) Point P4 in the AMARINTHOS area; and (E) Point P5 in the ALIVERI area, focusing on the warmest day of the simulations (August 2 at 15:00 p.m.).

August 27th in the year 2016. At a depth of 8 meters, point P2 exhibits the highest water velocity in comparison to the other two points, P4 and P5 which are located at depths of 8 and 13 meters, respectively.

The relationship between density σ and density ρ may be expressed as follows:

$$\rho = 1000 + \sigma\left(\mathrm{kg}/\mathrm{m}^3\right) \tag{1}$$

The degree of stratification is typically calculated as follows:

$$\varepsilon(z) = -\left(g/\rho_b\right)\cdot\left(\rho_s - \rho_b/H\right) \tag{2}$$

where $\varepsilon(z)$ is the stratification gradient, ρ_s is the surface density, ρ_b is the bottom density, H is the depth of water and g is the acceleration of gravity [30].

6.1. Dissolved Oxygen

In the comparative analysis of dissolved oxygen concentrations within the water column at all control points shown on the map in **Figure 6**, including:

1) Point P1 located in the region of POLITIKA,

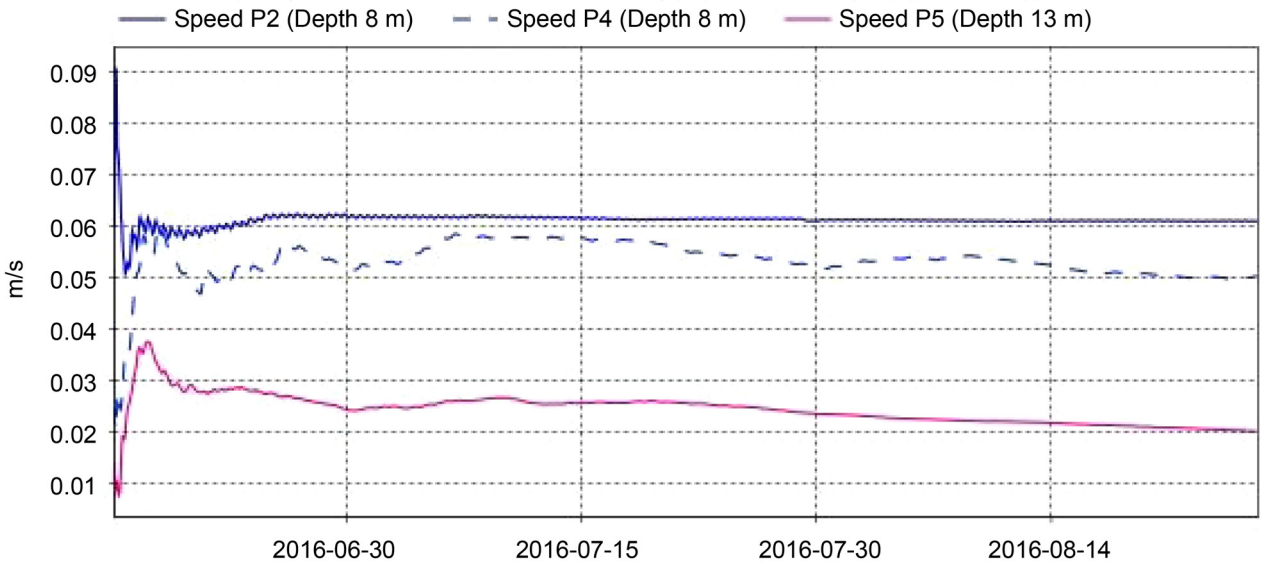

Figure 10. A contrast of daily water velocities during the hottestphase of the simulations, spanning from June 15 to August 27, as calculated using the AEM3D software for both the 2016 model and the hypothetical climate scenario (abbreviated as H.C.S.). This comparison is made for two specific locations: at Point P1 in the POLITIKA area within the 17 m bottom layer and at Point P4 in the AMARINTHOS area within the 8 m bottom layer.

2) Point P2 located in the region of CHALKIS,
3) Point P3 located in the region of ERETRIA,
4) Point P4 located in the region of AMARINTHOS, and
5) Point P5 located in the region of ALIVERI,

the assessment was carried out for the hottest phase in both simulations, spanning from June 15th to August 27th, specifically in the bottom layers of these points, at depths of 17 meters, 8 meters, 8 meters, 8 meters, and 13 meters, respectively, as illustrated in Figures 11(A)-(E). The findings reveal that, during the warm period in the theoretical climate setting, the dissolved oxygen concentrations in the bottom layers of all control points are slightly lower in comparison to those in the year 2016. The reductions in concentration are as follows: 0.02 mg/L for point P1, 0.05 mg/L for point P2, 0.09 mg/L for point P3, 0.07 mg/L for point P4, and 0.07 mg/L for point P5. These results align with expectations, as it is known that dissolved oxygen concentration is significantly influenced by water temperature. Higher water temperatures lead to lower oxygen content in the water, as evidenced by Figure 9, which illustrates higher temperatures throughout the water column at all control points (P1, P2, P3, P4, and P5) on the warmest day of the simulations in the theoretical climate setting by comparison with that of the year 2016. Specifically, when water temperature rises, the increased energy of gas and water molecules weakens the molecular interactions between water molecules and oxygen molecules, causing oxygen to escape and consequently reducing its concentration in the water.

6.2. Biological Oxygen Demand

In Figures 12(A)-(E), the concentrations of biochemical oxygen demand (BOD)

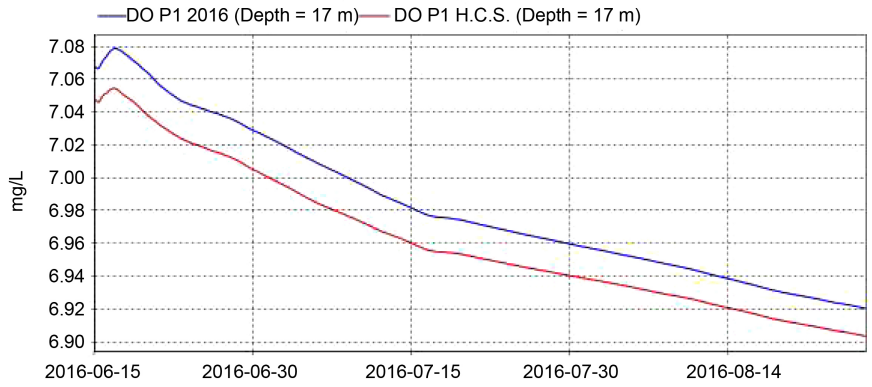
DO P1 2016 (Depth = 17 m)
DO P1 H.C.S. (Depth = 17 m)
mg/L
7.08
7.06
7.04
7.02
7.00
6.98
6.96
6.94
6.92
6.90
2016-06-15
2016-06-30
2016-07-15
2016-07-30
2016-08-14

(A)

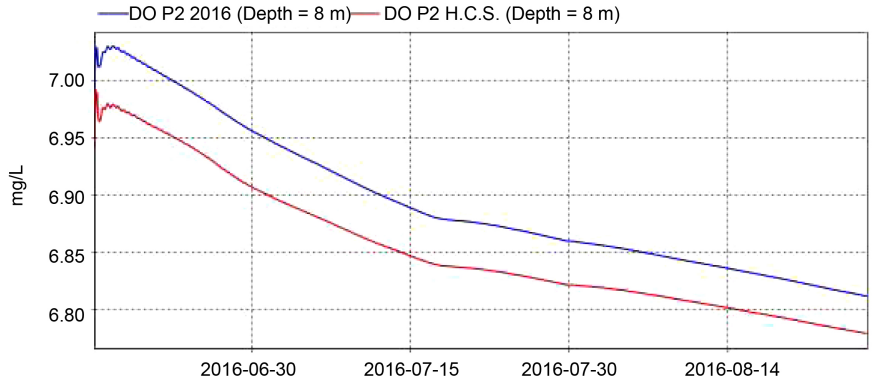
DO P2 2016 (Depth = 8 m)
DO P2 H.C.S. (Depth = 8 m)
mg/L
7.00
6.95
6.90
6.85
6.80
2016-06-30
2016-07-15
2016-07-30
2016-08-14

(B)

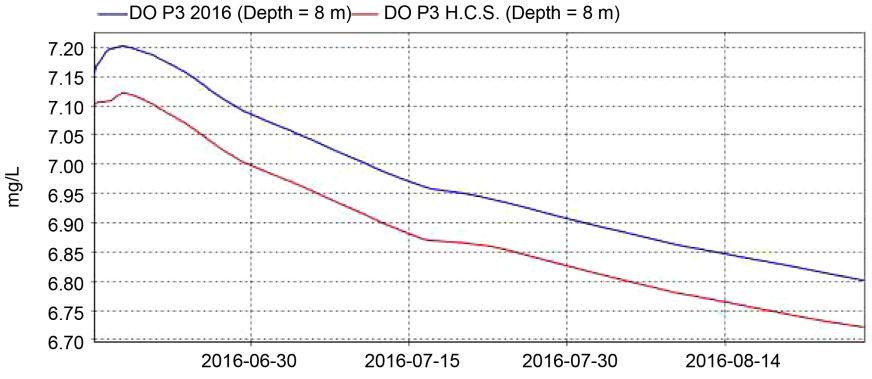
DO P3 2016 (Depth = 8 m)
DO P3 H.C.S. (Depth = 8 m)
mg/L
7.20
7.15
7.10
7.05
7.00
6.95
6.90
6.85
6.80
6.75
6.70
2016-06-30
2016-07-15
2016-07-30
2016-08-14

(C)

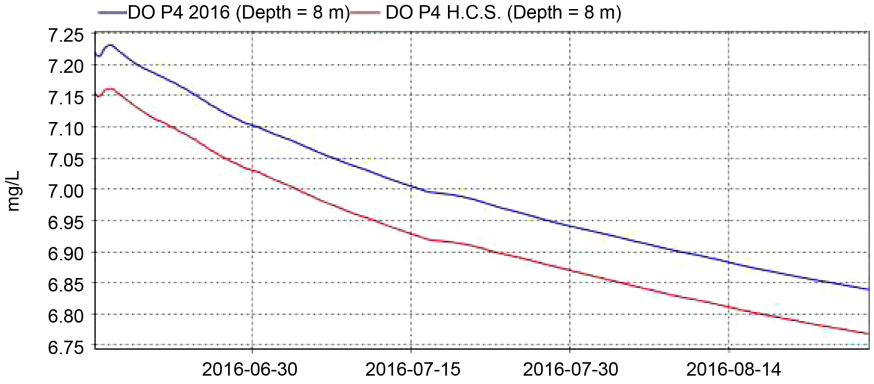
DO P4 2016 (Depth = 8 m)
DO P4 H.C.S. (Depth = 8 m)
mg/L
7.25
7.20
7.15
7.10
7.05
7.00
6.95
6.90
6.85
6.80
6.75
2016-06-30
2016-07-15
2016-07-30
2016-08-14

(D)

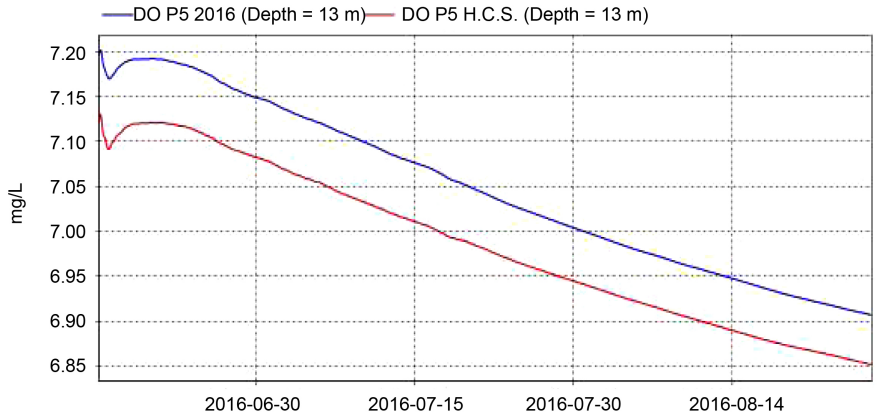

(E)

Figure 11. A comparative analysis of dissolved oxygen (DO) concentrations in (mg/L) during the hottestphase of the simulations, spanning from June 15 to August 27. These values are derived from the AEM3D software for both the year 2016 and the hypothetical climate scenario (abbreviated as H.C.S.). The comparisons are made at various points: (A) Point P1 in the POLITIKA area within the 8 m deep seabed layer; (B) Point P2 in the CHALKIS area within the 8 m deep seabed layer; (C) Point P3 in the ERETRIA area within the 8 m deep seabed layer; (D) Point P4 in the AMARINTHOS area within the 8 m deep seabed layer; and (E) Point P5 in the ALIVERI area within the 13 m deep seabed layer.

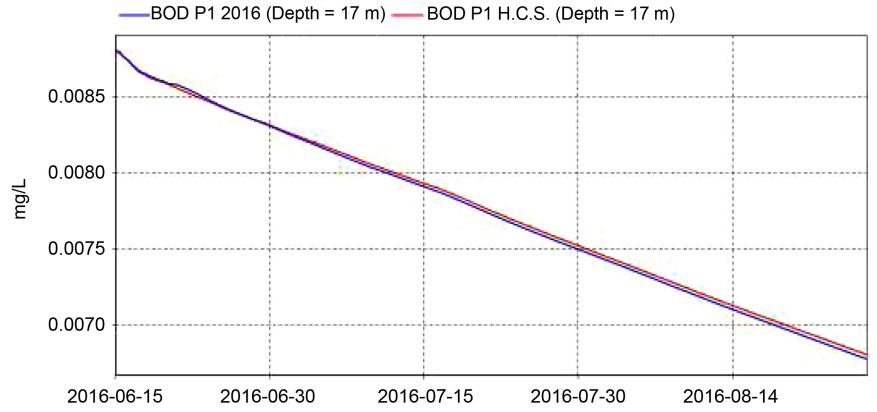

(A)

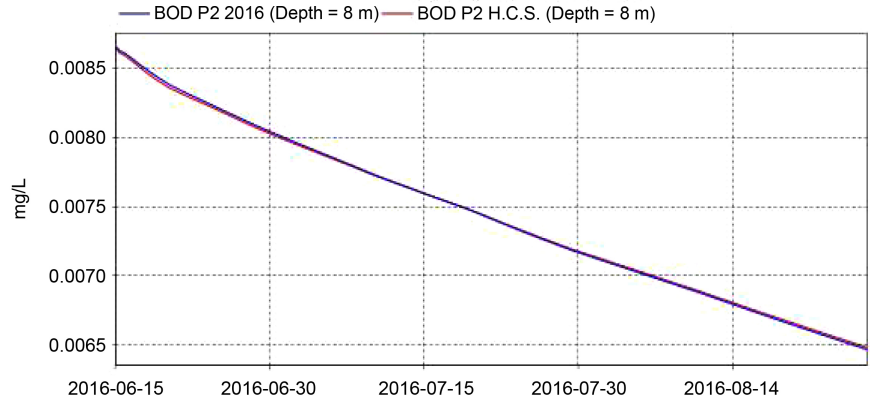

(B)

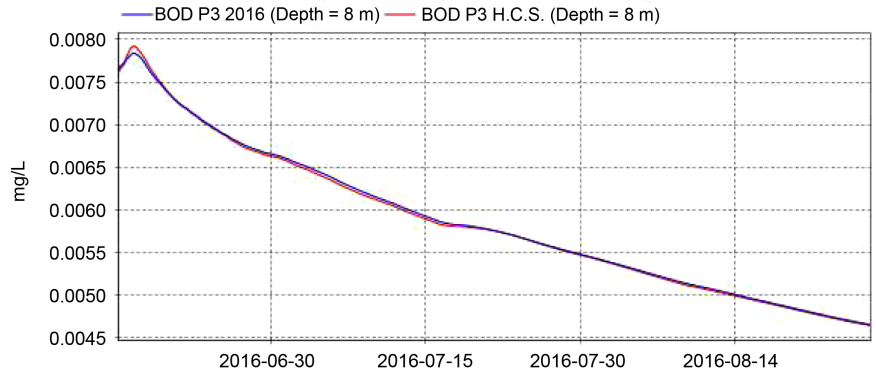

(C)

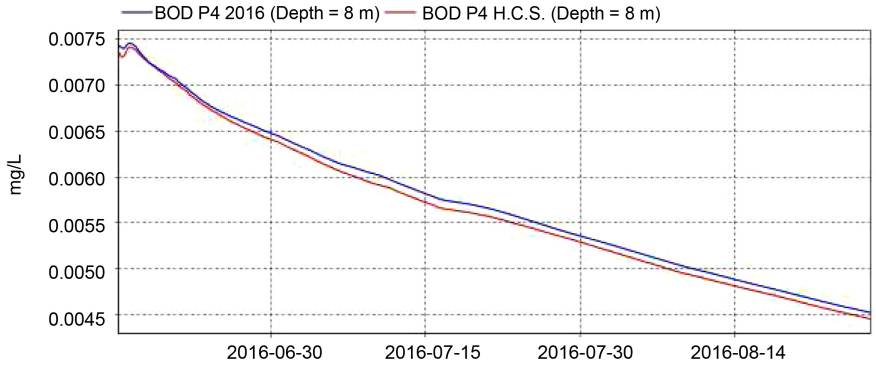

(D)

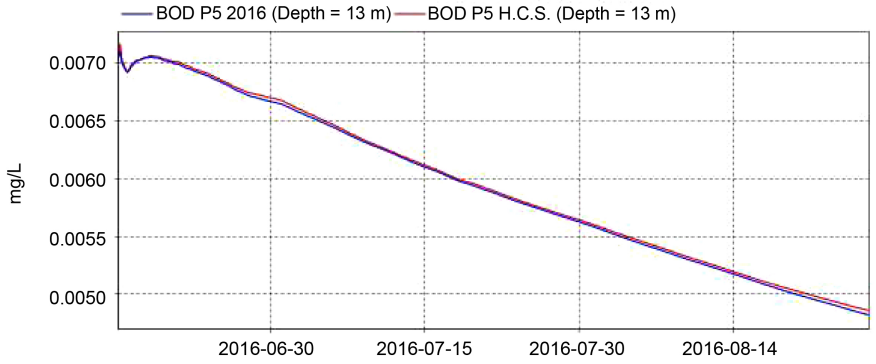

(E)

Figure 12. A comparative examination of the biochemically required oxygen (BOD) concentrations in (mg/L) during the hottest phase of the simulations, occurring from June 15 to August 27. These values are generated using the AEM3D software for both the year 2016 and the hypothetical climate scenario (abbreviated as H.C.S.). The comparisons are conducted at multiple locations: (A) Point P1 in the POLITIKA area within the 8 m deep seabed layer; (B) Point P2 in the CHALKIS area within the 8 m deep seabed layer; (C) Point P3 in the ERETRIA area within the 8 m deep seabed layer; (D) Point P4 in the AMARINTHOS area within the 8 m deep seabed layer; and (E) Point P5 in the ALIVERI area within the 13 m deep seabed layer.

in the 17 m, 8 m, 8 m, 8 m and 13 m deep seabed layers at P1, P2, P3, P4 and P5 respectively for both climate scenarios during the hottest phase of the simulations from 15 June to 27 August have been plotted. In the 13 m deep seabed

layer of point P5, where in this and in point P3, the most pronounced increase in stratification in comparison with the other points has been noted, as observed from Figure 12(E):

A small increase in the concentration of biochemically required oxygen in the model of the climate scenario of the hypothesis in comparison to the 2016-year model, during the hottest period of the simulations from 15 June to 27 August. This effect is apparently due to the restriction of the diffusion of organic loads in the upper layers of the water column, from the stronger stratification observed at this point. While in both simulations, that of the base year 2016 and that of the hypothetical scenario, according to Figure 11 and Figure 12, overall for all control points P1, P2, P3, P4 and P5, a downward trend with time is observed for both the concentration of biochemically required oxygen and that of dissolved oxygen. This result is to be expected since dissolved oxygen is the oxidizing agent for the removal of organic carbon, which is quantitatively represented by BOD.

6.3. Nutrients

From Figures 13(A)-(C) and Figures 14(A)-(C) below, it can be seen that in the 8 m, 8 m and 13 m deep seabed layers of control points P3, P4 and P5, located in the areas of South Euboean Gulf, ERETRIA, AMARINTHOS and ALIVERI respectively, as depicted on the map in Figure 6 and listed in Table 1, the nutrients. total nitrogen, nitrate nitrogen, phosphates and total phosphorus show higher concentrations, in the hottest period of the simulations, spanning from June 15th to August 27th for the theoretical climate setting in comparison with that of the base year 2016. Specifically, the resulting increases in nutrient concentrations in (mg/L) are:

1) For nitrate nitrogen (NO_3-N), 0.00015 at P3, 0.0002 at P4 and 0.0001 at P5.

2) For total nitrogen (Total N), 0.00015 at P3, 0.0002 at P4 and 0.00004 at P5.

3) For phosphates (PO_4), 0.00005 at P3, 0.00005 at P4 and 0.00002 at P5.

4) For total phosphorus (Total P), 0.00005 at P3, 0.00005 at P4 and 0.00002 at P5.

This is obviously due to the limitation of their vertical mixing, since due to the increased stratification during the warm season, in the theoretical climate setting in comparison with the base year 2016, their ascent to the upper water layers is hindered [31].

An illustrative example is shown in Figure 15 below, which compares the daily changes in ammonium, nitrate and total nitrogen concentrations obtained between the 2016 base year models and the theoretical climate setting in the 8 m deep seabed layer at control point P3, during the hottest simulation time period spanning from June 15th to August 27th. In this figure, it can be seen that as the ammonium concentration values stabilize, the nitrate concentration values increase, due to the nitrification process that takes place, during which NH_4-N is converted to NO_3-N. In the same time period, as seen in Figure 11(c), there is a

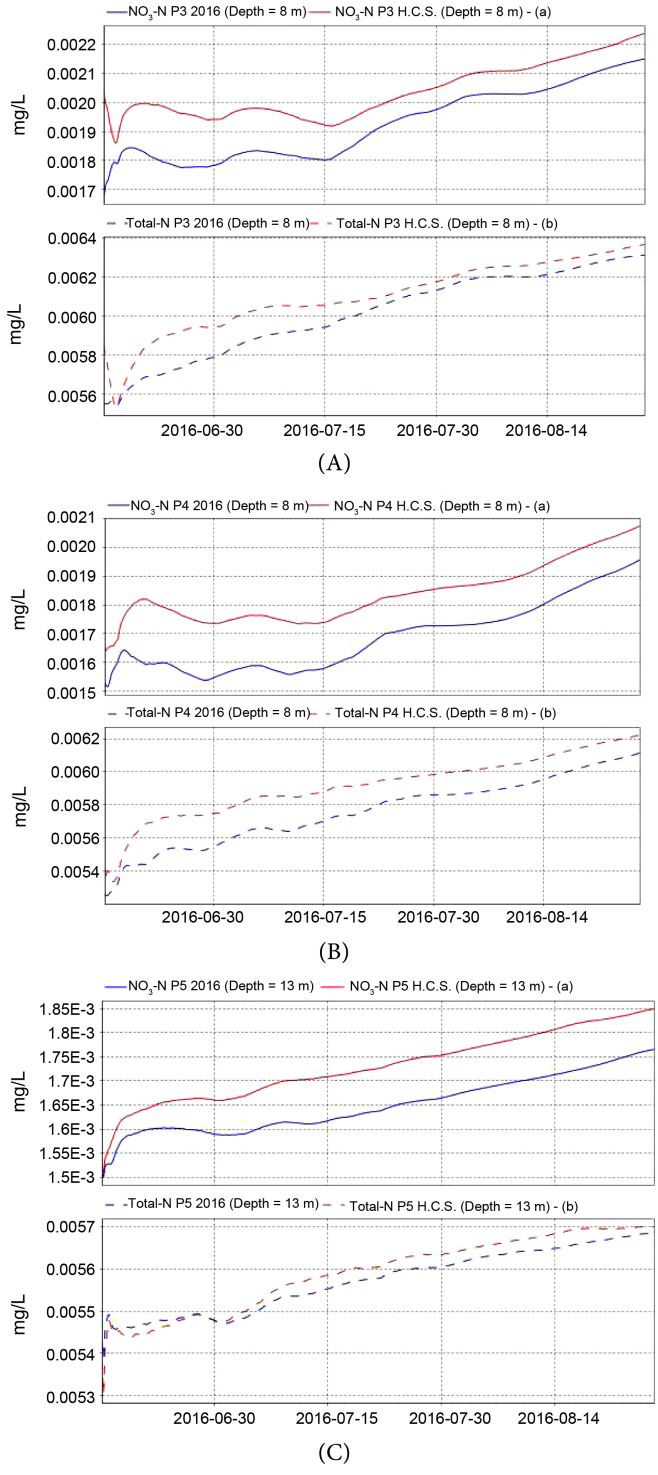

Figure 13. A comparative analysis of the concentration in (mg/L) for (a) Nitrate nitrogen (NO_3-N) and (b) Total nitrogen (Total N) during the hottestphase of the simulations, spanning from June 15 to August 27. These values are derived from the AEM3D software for both the year 2016 and the hypothetical climate scenario (abbreviated as H.C.S.). The comparisons are conducted at three specific points: (A) Point P3 in the ERETRIA area within the 8 m deep seabed layer; (B) Point P4 in the AMARINTHOS area within the 8 m deep seabed layer; and (C) Point P5 in the ALIVERI area within the 13 m deep seabed layer.

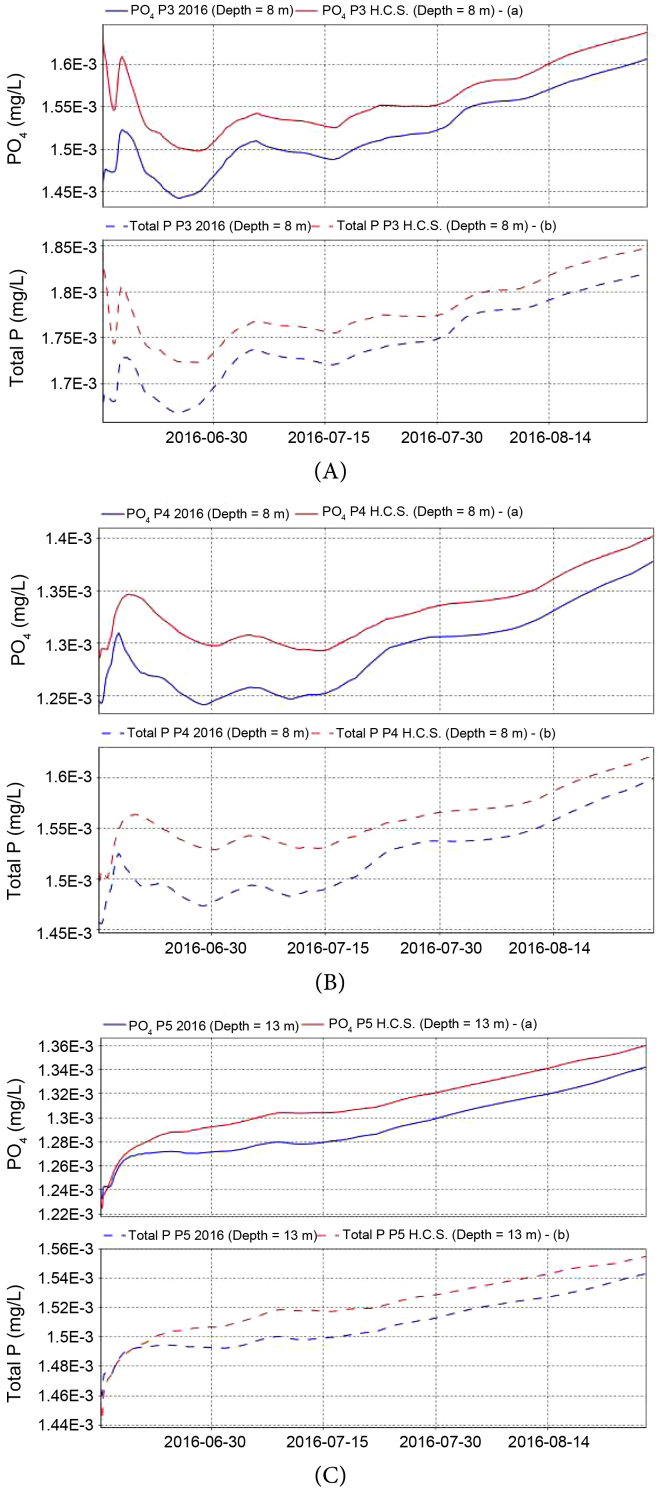

Figure 14. A comparative analysis of the concentration in (mg/L) of (a) Phosphite ions (PO_3) and (b) Total phosphorus (Total P), during the hottestphase of the simulations, spanning from June 15 to August 27, as obtained with the AEM3D software for the year 2016 and for the year of the hypothetical climate scenario (for short H.C.S.). These comparisons are conducted at three specific points: (A) Point P3 of the ERETRIA area in the 8 m deep seabed layer; (B) Point P4 of the AMARINTHOS area in the 8 m deep seabed layer; and (C) Point P5 of the ALIVERI area in the 13 m deep seabed layer.

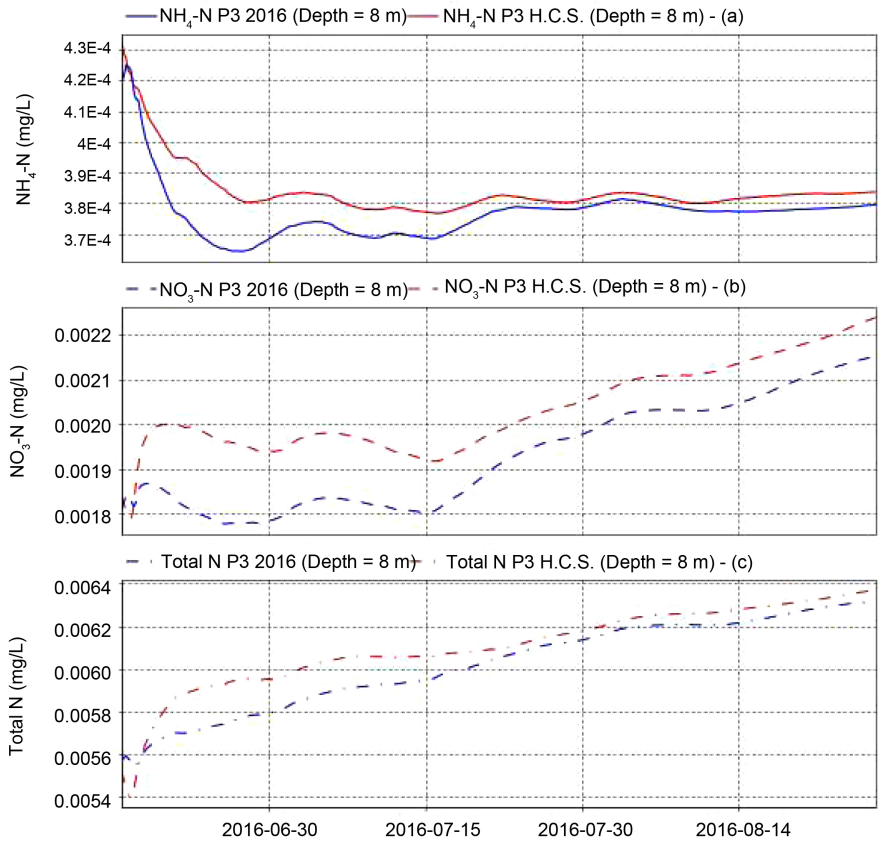

Figure 15. A comparative analysis of the concentration in (mg/L) for (A) Ammonium nitrogen (NH_4-N); (B) Nitrate nitrogen (NO_3-N); and (C) Total nitrogen (Total N) during the hottestphase of the simulations, spanning from June 15 to August 27. These values are derived from the AEM3D software for both the year 2016 and the hypothetical climate scenario (abbreviated as H.C.S.). The comparison focuses on point P3 in the ERETRIA area within the 8 m deep seabed layer.

decreasing trend in the dissolved oxygen concentration in the results of both simulations, that of the base year 2016 and that of the climate scenario of the hypothesis. This is due both to the removal of organic carbon with dissolved oxygen as the oxidant, and to the nitrification process that takes place, in which dissolved oxygen is still the oxidant, but with fewer requirements than the nitrification process.

6.4. Total Coliforms

Figures 16(A)-(E) below illustrate the comparison of daily changes in Total Coliforms concentrations during the hottest simulation time period spanning from June 15th to August 27th, contained in the urban wastewater discharged to the computational site via the subsea pipelines shown in Figure 6. Figure 16 shows overall that the concentrations of Total Coliforms in the 17 m, 8 m, 8 m, 8 m and 13 m deep seabed layers at all control points P1, P2, P3, P4 and P5 respectively, are lower in the case of the simulation of the climate scenario of the hypothesis in comparison with those obtained from the simulation with the climatic data of

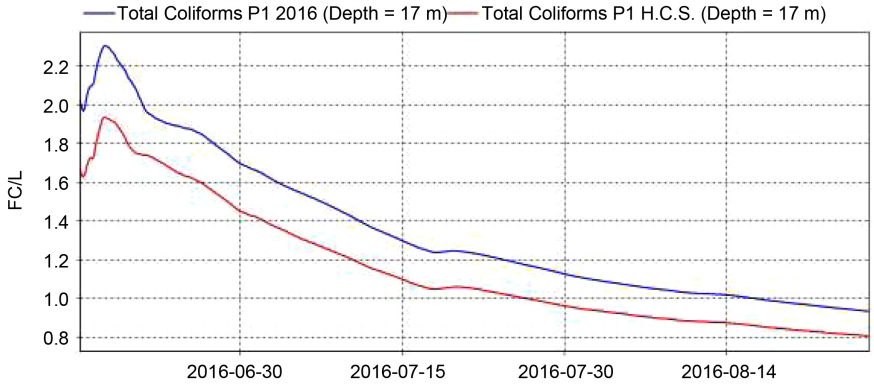
Total Coliforms P1 2016 (Depth = 17 m)
Total Coliforms P1 H.C.S. (Depth = 17 m)
FC/L
2.2
2.0
1.8
1.6
1.4
1.2
1.0
0.8
2016-06-30
2016-07-15
2016-07-30
2016-08-14

(A)

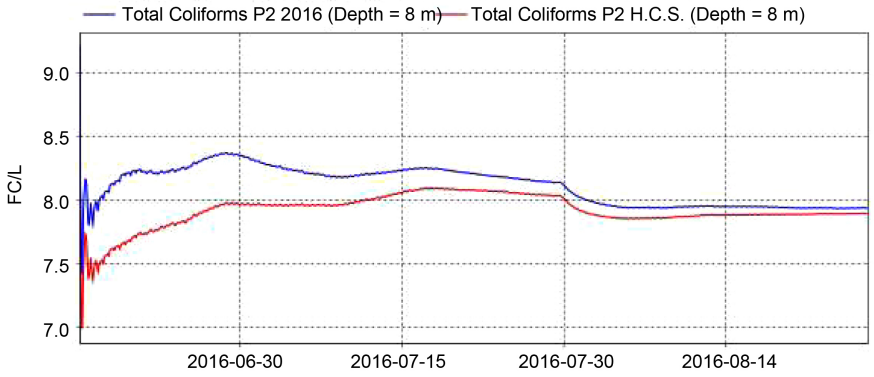
Total Coliforms P2 2016 (Depth = 8 m)
Total Coliforms P2 H.C.S. (Depth = 8 m)
FC/L
9.0
8.5
8.0
7.5
7.0
2016-06-30
2016-07-15
2016-07-30
2016-08-14

(B)

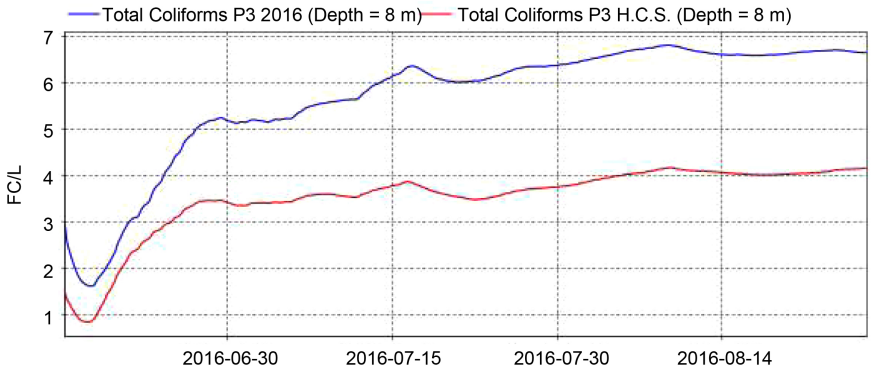
Total Coliforms P3 2016 (Depth = 8 m)
Total Coliforms P3 H.C.S. (Depth = 8 m)
FC/L
7
6
5
4
3
2
1
2016-06-30
2016-07-15
2016-07-30
2016-08-14

(C)

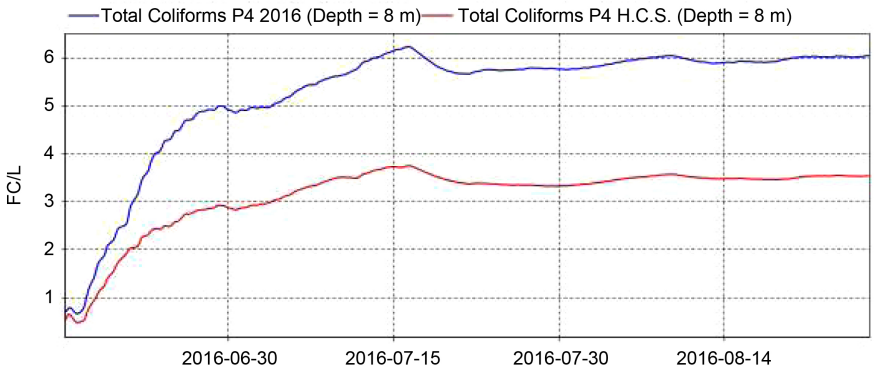
Total Coliforms P4 2016 (Depth = 8 m)
Total Coliforms P4 H.C.S. (Depth = 8 m)
FC/L
6
5
4
3
2
1
2016-06-30
2016-07-15
2016-07-30
2016-08-14

(D)

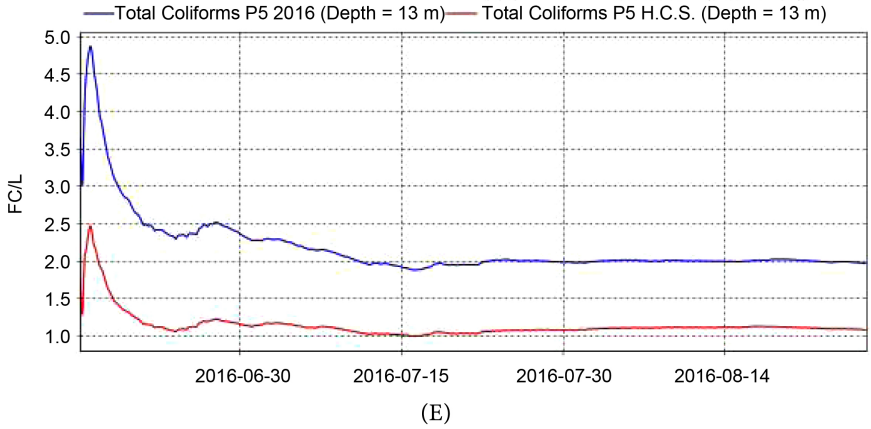

Figure 16. Comparison of Total Coliforms concentration in (FC/L) during the hottest-phase of the simulations spanning from June 15 to August 27, as obtained with the AEM3D software for the year 2016 and for the year of the hypothetical climate scenario (for short H.C.S.). These comparisons are conducted at the following points: (A) Point P1 in the POLITIKA area in the 8 m deep layer of seabed layer; (B) Point P2 in the CHALKIS area in the 8 m deep seabed layer; (C) Point P3 in the ERETRIA area in the 8 m deep seabed layer; (D) Point P4 in the AMARINTHOS area in the 8 m deep seabed layer and (E) Point P5 in the ALIVERI area in the 13 m deep seabed layer.

the year 2016. In particular, differences of up to 0.2 FC/mL at P1, 0.38 FC/mL at P2, 2.65 FC/mL at P3, 2.5 FC/mL at P4 and 1.0 FC/mL at P5 are obtained. This is obviously due to the lower dissolved oxygen concentration levels found in the lower layers of all control points in the case of the simulated climate scenario of the hypothesis against that of 2016, which are illustrated in **Figure 11**. Lower dissolved oxygen levels lead to higher mortality of a significant proportion of Total Coliforms.

6.5. Sediment

Figure 17 below shows (a) the mass in (g/m^2) and (b) the deposition thickness in (m) of the sediment of suspended solid particles from urban sewage discharged into the marine environment from the five diffusers simulated in the computational domain, during the hottest period of the simulations from 15 June to 27 August, for the theoretical climate setting and that of the year 2016. **Figures 17(A)-(C)** depict the above parameters in the 8 m, 8 m and 13 m deep seabed layers of control points P3, P4 and P5, located in the areas of South Euboean Gulf, ERETRIA, AMARINTHOS and ALIVERI respectively, as shown on the map in **Figure 6** and listed in **Table 1**. For these three areas, higher amounts of sediment on the bottom are obtained for the theoretical climate setting, in comparison to that of the year 2016. Specifically, the resulting differences are 0.0005 g/m^2 at point P3, 0.0005 g/m^2 at point P4 and 0.0004 g/m^2 at point P5. This is due to the inhibition of suspended solid particles to rise to the upper water layers, due to the increased stratification and density variation in the water column at these points, as has been established in **Figure 9**, for the case of the theoretical

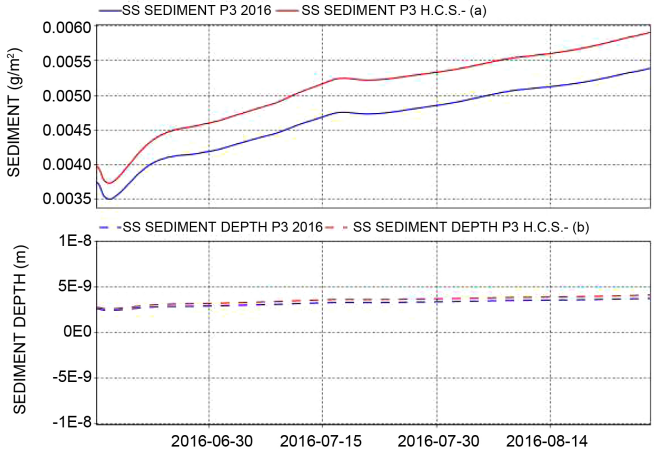

(A)

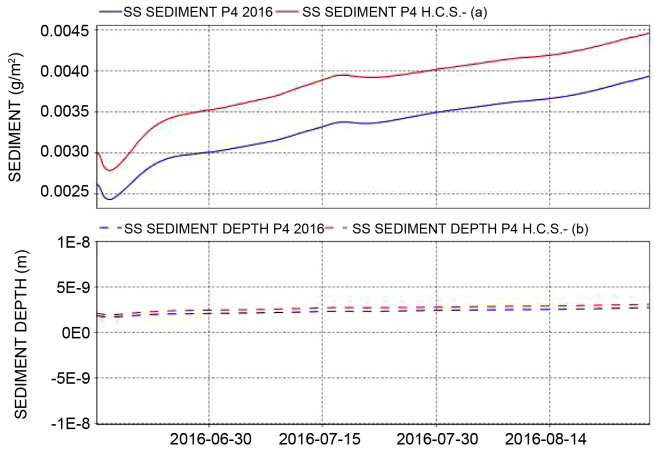

(B)

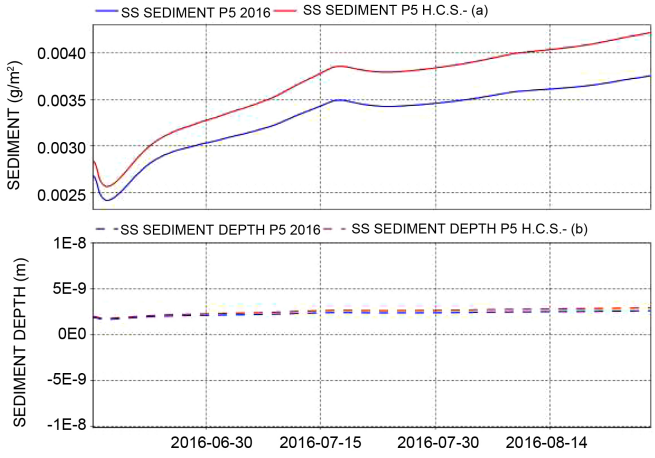

(C)

Figure 17. A contrast analysis of sediment suspended solid particles, including (a) Mass in (g/m^2) and (b) Thickness in (m), during the hottest phase of the simulations spanning from June 15 to August 27. These data were obtained using the AEM3D software for both the year 2016 and the hypothetical climate scenario (abbreviated as H.C.S.). The comparison focuses on three locations: (A) Point P3 in the ERETRIA area within the 8 m deep seabed layer; (B) Point P4 in the AMARINTHOS area within the 8 m deep seabed layer; and (C) Point P5 in the ALIVERI area within the 13 m deep seabed layer.

climate setting in comparison to that of the 2016 base year.

7. Discussion

As stated in paragraphs As stated in paragraphs 6.3 and 6.5, in areas of the South Euboean gulf that are more stratified than the rest, according to **Figures 9(A)-(E)**, during the warm season in the theoretical climate setting in comparison to that of the base year 2016, the results of the concentrations of nutrients and the conservative pollutants of the urban wastewater from the diffusers simulated in the computational domain are worse in the theoretical climate setting. Specifically, in the bottom water layers of points P3, P4 and P5 located in South Euboean gulf as depicted in **Figure 6**, the concentrations of ammonium, nitrate, total nitrogen, phosphate, total phosphorus and suspended solid particles in the sediment, according to **Figure 13**, **Figure 14** and **Figure 17**, are higher in the theoretical climate setting, in comparison to the base year 2016, during the hottest period of the two climate scenarios, from 15 June to 27 August.

Figure 18 and **Figure 19** below show the changes in temperature and water density as well as water age (water residence time), in the bottom layers of representative areas of the South Euboean gulf, where higher stratification has been observed during the warm period in comparison to the rest, in the theoretical climate setting in comparison to that of the base year 2016. In comparison, at control points P3 and P5 during the selected warm period from 15 June to 27 August of the two climate scenarios, the following results are obtained:

- Higher water temperatures, resulting in lower water density values for the theoretical climate setting in comparison to those of the base year, in the seabed layers of control points P3 and P5, according to **Figure 18**.
- Longer water residence times in the lower seabed layers of P3 and P5 of 12 and 11 days respectively, according to **Figure 19(A)** and **Figure 19(B)** in the theoretical climate setting in comparison to the base year 2016, during the hottest period.

According to **Figure 18(A)** and **Figure 18(B)** below, it would be expected that there would be shorter residence times of water in the lower seabed layers of control points P3, P4 and P5, due to its lower density in the case of the climate scenario of the hypothesis and thus lower concentrations of urban wastewater pollutants. However, from **Figure 19(A)** and **Figure 19(B)**, longer residence times of the water in the seabed layers of the points of the South Euboean Gulf, as can be seen at points P3 and P5. This leads to the conclusion that in the lower water layers of the southern Euboean Gulf points P3, P4 and P5 examined during the hottest period, the stronger stratification found at these points in the theoretical climate setting in comparison to the base year prevails, which creates conditions of slower water renewal and less favorable mixing of pollutants. Thus, higher concentrations of suspended solid particles and nutrients appear in the seabed layers of points P3, P4 and P5 of the southern Euboean Gulf in the theoretical climate scenario in comparison with the corresponding base year 2016.

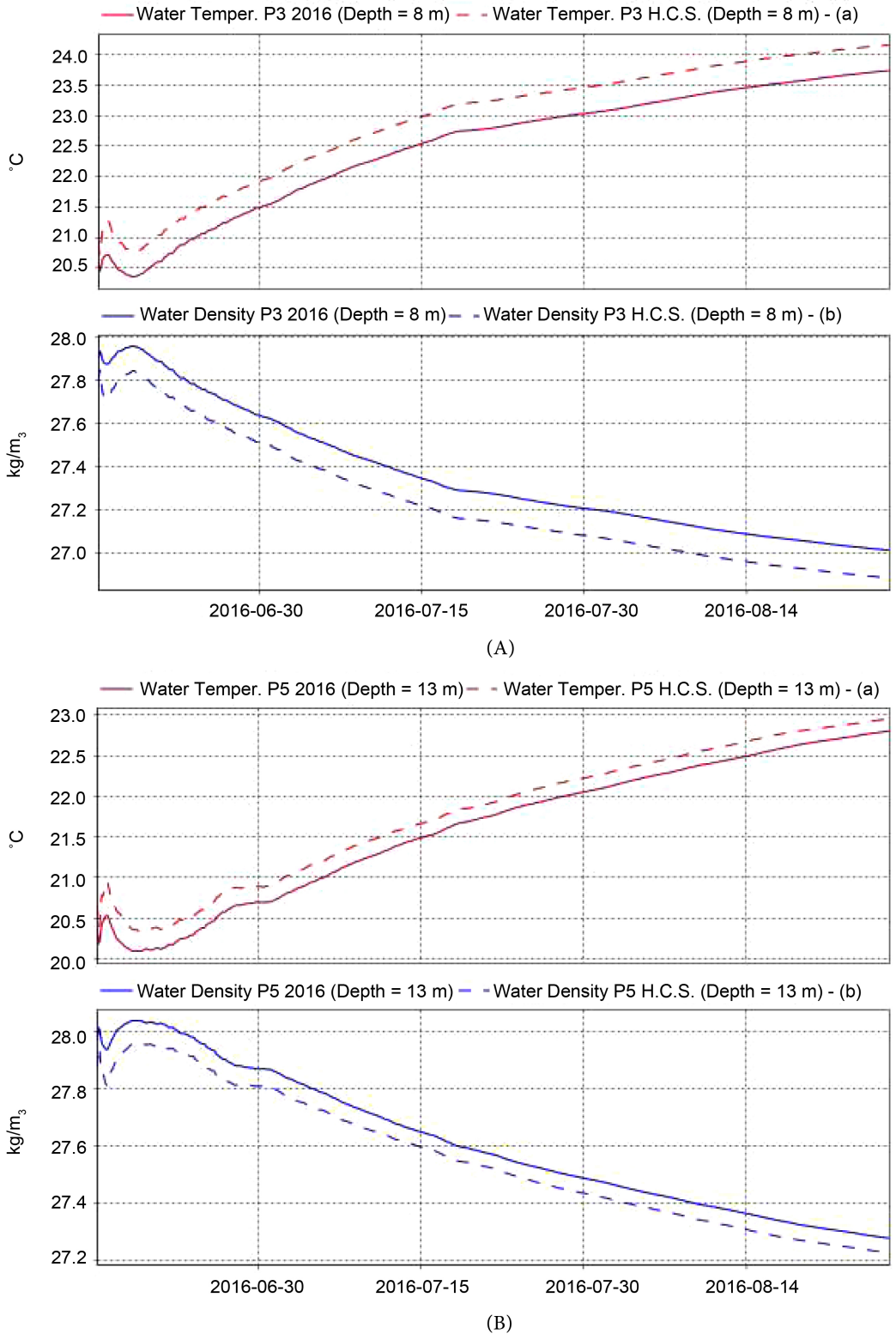

Figure 18. A comparative analysis of (a) water temperature in ˚C and (b) water density σ in Kg/m^3 during the hottestphase of the simulations, spanning from June 15 to August 27. The data is obtained using the AEM3D software for the year 2016 and the hypothetical climate scenario (H.C.S.). The comparison is made at two points: (A) Point P3 in the ERETRIA area, at a seabed depth of 8 m; and (B) Point P5 in the ALIVERI area, at a seabed depth of 13 m.

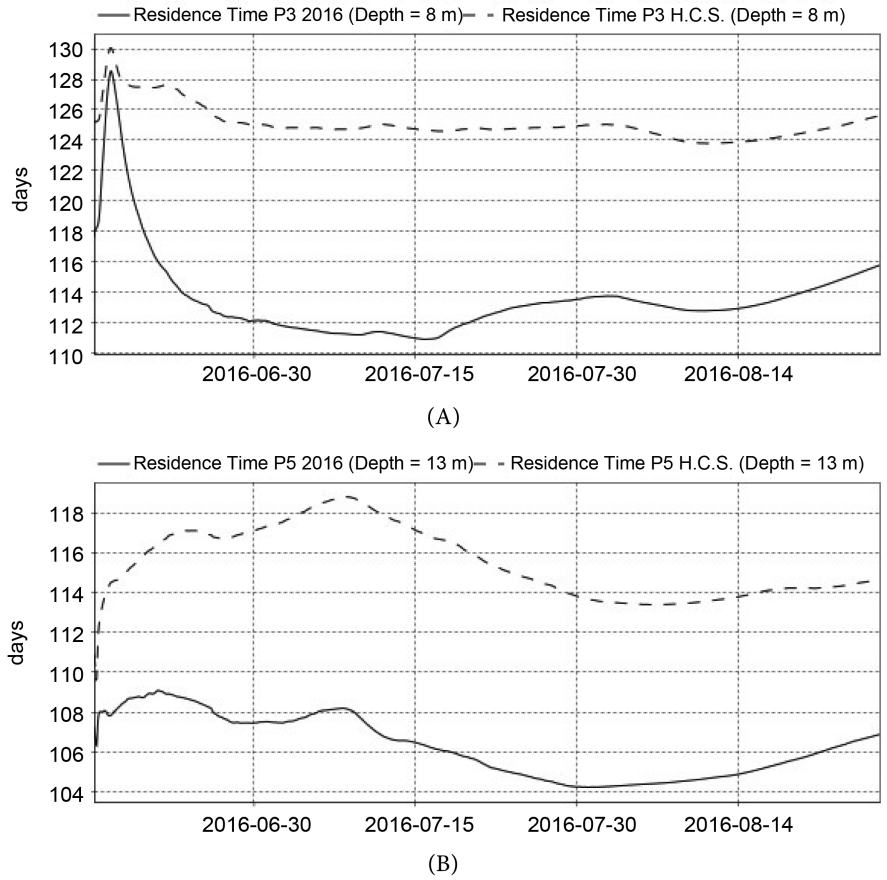

Figure 19. A comparative analysis of water age in (days), during the hottest phase of the simulations, ranging from 15 June to 27 August, as obtained with the AEM3D software for the year 2016 and for the year of the hypothetical climate scenario (H.C.S. for short). The comparison is made at two points: (A) Point P3 of the ERETRIA area in the 8 m deep seabed layer and (B) Point P5 of the ALIVERI area in the 13 m deep seabed layer.

8. Conclusions

In the present study, computational simulations were conducted to model the hydrodynamic circulation in the Euboean Gulf using the 3-Dimensional coupled Hydrodynamic-Aquatic Ecosystem Model AEM3D. This model represents an advancement of the ELCOM-CAEDYM software and is capable of accounting for various factors, including the influence of tides, the Coriolis force, and climatic conditions.

Two simulations were conducted for this study. One utilized climate data obtained from regional measurement stations in 2016, while the other employed a theoretical climate setting. In the hypothetical scenario, a time series for air temperature was employed, featuring values that were on average 1.5˚C higher than those recorded in the base year 2016. In a general comparison of the results, it was observed that, in principle, the future climate scenario yielded higher water column temperatures at all points of interest. This increase was attributed to the rise in air temperature. Regarding the water column density in the lower water layers of most coastal points of interest, an augmentation in stratification was

detected during the warm period in the simulations of the theoretical climate setting when compared to those of the base year 2016. However, there were exceptions in areas where local conditions, such as heightened water velocities at point P2 due to the tides in the Euripus Strait, resulted in uniformity in water density variations between the two climate scenarios.

The results also showed a decrease in dissolved oxygen concentrations in the bottom layers of all points of interest for the hypothetical climate, by increasing the water column temperature caused by the increase in air temperature.

The pollutant loads from the urban wastewater diffusers installed in the area, both for nutrients (N and P) and for the conservative pollutants, suspended solid particles, resulted in higher concentrations for the climate scenario of the hypothesis in comparison with that of the 2016 base year, in the lower layers of all POIs where increased stratification was observed.

The findings discussed above lead to the conclusion that the anticipated slight increase in water column stratification in various parts of the Euboean Gulf in the future, assuming greenhouse gas limitations are not imposed, will pose additional challenges to the vertical mixing of sea masses, especially in the coastal regions of the South Euboean Gulf. Consequently, this could impact the dispersion and mixing of pollutants discharged into the coastal marine environment from human activities such as urban wastewater disposal. These observations lay the foundation for further research aimed at developing strategies to mitigate stratification in these areas of interest while maintaining water quality, particularly in the absence of substantial reductions in greenhouse gas emissions, which play a significant role in driving global air temperature increases.

Acknowledgments

The writer extends heartfelt gratitude to God Almighty and deeply appreciates Dr. Panagiotis Angelidis, Professor of the Department of Civil Engineering at the School of Engineering of the Democritus University of Thrace, for providing the opportunity to undertake this Postdoctoral Research. The writer also expresses sincere appreciation to their family for their unwavering support and, lastly, extends thanks to Dr. Ioannis Karamouzis for his invaluable spiritual support.

Conflicts of Interest

The authors affirm that there are no conflicts of interest pertaining to the publication of this paper.

References

[1] Pirooznia, M., Emadi, S.R. and Alamdari, M.N. (2016) The Time Series Spectral Analysis of Satellite Altimetry and Coastal Tide Gauges and Tide Modeling in the Coast of Caspian Sea. *Open Journal of Marine Science*, **6**, 258-269. http://dx.doi.org/10.4236/ojms.2016.62021

[2] Onguene, R., *et al.* (2015) Overview of Tide Characteristics in Cameroon Coastal

Areas Using Recent Observations. *Open Journal of Marine Science*, **5**, 81-98. http://dx.doi.org/10.4236/ojms.2015.51008

[3] Manasrah, R. (2013) Tide Variation and Signals during 2000-2004 in the Northern Gulf of Aqaba, Red Sea. *Natural Science*, **5**, 1264-1271. http://dx.doi.org/10.4236/ns.2013.512154

[4] Pous, S., Carton, X. and Lazure, P. (2012) A Process Study of the Tidal Circulation in the Persian Gulf. *Open Journal of Marine Science*, **2**, 131-140. http://dx.doi.org/10.4236/ojms.2012.24016

[5] Vanlede, J., Coen, L. and Deschamps, M. (2014) Tidal Prediction in the Sea Scheldt (Belgium) Using a Combination of Harmonic Tidal Prediction and 1D Hydraulic Modeling. *Natural Resources*, **5**, 627-633. http://dx.doi.org/10.4236/nr.2014.511055

[6] Jeyar, M., Chaabelasri, E.M. and Salhi, N. (2015) Computational Modeling of Tidal Effect on Wastewater Dispersion in Coastal Bays, Case of Tangier's Bay (Morocco). *Journal of Materials and Environmental Science*, **6**, 1715-1718.

[7] Vaselali, A. (2009) Modeling of Brine Waste Discharges Spreading under Tidal Currents. *Journal of Applied Sciences*, **9**, 3454-3468. https://doi.org/10.3923/jas.2009.3454.3468

[8] Abualtayef, M., Al-Najjar, H., Mogheir, Y. and Seif, A.K. (2016) Numerical Modeling of Brine Disposal from Gaza Central Seawater Desalination Plant. *Arabian Journal of Geosciences*, **9**, Article No. 572. https://doi.org/10.1007/s12517-016-2591-7

[9] Livieratos, E. (1980) The M_2 Sea-Tidal Propagation in the Evoikos Bay. *Technika Chronika*, **5**, 48-55.

[10] Eginitis, D. (1929) The Problem of the Tides of Euripus. *Astronomische Nachrichten*, **236**, 321-328. https://doi.org/10.1002/asna.19292361904

[11] Endros, A. (1915) Die Gezeiten, Seiches und Stromungen des Meeresbei Aristoteles. Sitzungsberichte der Bayerischen Akademie der Wissenschafter (math.-phys.), Kl, 99.

[12] Sterneck, R.V. (1916) Zur Theorie der Euripus-Stromungen. Sitzungsberichte der Akademie der Wissenschafter in Wien (Abt. IIa).

[13] Defant, A. (1961) Physical Oceanography Volume II. Pergamon Press, London.

[14] Tsimplis, M.N. (1997) Tides and Sea-Level Variability at the Strait of Euripus. *Estuarine, Coastal and Shelf Science*, **44**, 91-101. https://doi.org/10.1006/ecss.1996.0128

[15] Wöppelmann, G. and Marcos, M. (2012) Coastal Sea Level Rise in Southern Europe and the Non-Climate Contribution of Vertical Land Motion. *Journal of Geophysical Research*, **117**, C01007. https://doi.org/10.1029/2011JC007469

[16] Ferrarin, C., Bellafiore, D., Sannino, G., Bajo, M. and Umgiesser, G. (2018) Tidal Dynamics in the Inter-Connected Mediterranean, Marmara, Black and Azov Seas. *Progress in Oceanography*, **161**, 102-115. https://doi.org/10.1016/j.pocean.2018.02.006

[17] Tsimplis, M.N. and Shaw, G.P. (2010) Seasonal Sea Level Extremes in the Mediterranean Sea and at the Atlantic European Coasts. *Natural Hazards and Earth System Sciences*, **10**, 1457-1475. https://doi.org/10.5194/nhess-10-1457-2010

[18] Marcos, M., Tsimplis, M.N. and Shaw, A.G.P. (2009) Sea Level Extremes in Southern Europe. *Journal of Geophysical Research*, **114**, C01007. https://doi.org/10.1029/2008JC004912

[19] Poulos, S., Drakopoulos, P., Leontaris, S., Tsapakis, E. and Hatjiyianni, E. (2001) The Contribution of Tidal Currents in the Sedimentation of Strait of Avlida, South-

ern Evoikos Gulf, Greece. *Proceedings of the 9th International Congress*, Athens, 26-28 September 2001, 731-736.

[20] Kontoyiannis, H., Panagiotopoulos, M. and Soukissian, T. (2015) The Euripus Tidal Stream at Halkida/Greece: A Practical, Inexpensive Approach in Assessing the Hydrokinetic Renewable Energy from Field Measurements in a Tidal Channel. *Journal of Ocean Engineering and Marine Energy*, **1**, 325-335. https://doi.org/10.1007/s40722-015-0020-8

[21] Tsirogiannis, E., Angelidis, P. and Kotsovinos, N. (2019) Hydrodynamic Circulation under Tide Conditions at the Gulf of Evoikos, Greece. *Computational Water, Energy, and Environmental Engineering*, **8**, 57-78. https://doi.org/10.1007/s40722-015-0020-8

[22] Kopasakis, K.I., Georgoulas, A.N., Angelidis, P.B. and Kotsovinos, N.E. (2012) Simulation of the Long-Term Fate of Water and Pollutants, Transported from the Dardanelles Plume into the North Aegean Sea. *Applied Ocean Research*, **37**, 145-161. http://dx.doi.org/10.1016/j.apor.2012.04.007

[23] Kopasakis, K., Georgoulas, A., Angelidis P. and Kotsovinos, N. (2012) Numerical Modeling of the Long-Term Transport, Dispersion and Accumulation of Black Sea Pollutants into the North Aegean Coastal Waters. *Estuaries and Coasts*, **35**, 1530-1550. https://doi.org/10.1007/s12237-012-9540-9

[24] Spillman, C.M., Imberger, J., Hamilton, D.P., Hipsey, M.R. and Romero, J.R. (2007) Modelling the Effects of Po River Discharge, Internal Nutrient Cycling and Hydrodynamics on Biogeochemistry of the Northern Adriatic Sea. *Journal of Marine Systems*, **68**, 167-200. https://doi.org/10.1016/j.jmarsys.2006.11.006

[25] Alosairi, Y., Imberger, J. and Falconer, R.A. (2011) Mixing and Flushing in the Persian Gulf (Arabian Gulf). *Journal of Geophysical Research*: *Oceans*, **116**, C03029.

[26] Bird, D., Wain, D., Slavin, E., Zang, J., Luckwell, R. and Bryant, Lee D. (2021) Stratification in a Reservoir Mixed by Bubble Plums under Future Climate Scenarios. *Water*, **13**, Article No. 2467. https://doi.org/10.3390/w13182467

[27] Kotsovinos, N. (1987) The Problem of Pollution in the Gulf of Evoikos. In: *Proceedings of the International Scientific Conference* "*The City of Chalkida*", Company of Euboean Studies, Chalkida, 353-387.

[28] Skaloumpakas, K. (2011) Study of the Tidal Energy Potential at the Euripus Strait and Operating Modes through Tidal Turbine Installation. Degree Thesis, National Technical University of Athens, Athens.

[29] Tsirogiannis, E., Angelidis, P. and Kotsovinos, N. (2019) Mixing Characteristics under Tide, Mereological and Oceonografic Conditions in the Euboean Gulf Greece. *Computational Water, Energy, and Environmental Engineering*, **8**, 99-123. https://doi.org/10.4236/cweee.2019.84007

[30] Fischer, H.B., List, E.J., Koh, R., Imberger, J. and Brooks, N.H. (1979) Mixing in Inland and Coastal Waters. Academic Press, New York.

[31] Tsirogiannis, E. and Angelidis, P. (2023) The Impact of Climate Change on the Stratification of Coastal Areas of the Euboean Gulf and the Diffusion of Urban Wastewater in Them. *Computational Water, Energy, and Environmental Engineering*, **12**, 1-26. https://doi.org/10.4236/cweee.2023.123001